Tyler, G. L., Eshleman, V. R., Anderson, J. D., Levy, G. S., Lindal, G. F., Wood, G. E., and Croft, T. A. 1982. Radio science with Voyager 2 at Saturn: Atmosphere and ionosphere and the masses of Mimas, Tethys, and Iapetus. *Science* 215:553–558.

Ward, W. 1981. Solar nebula dispersal and the stability of the planetary system. *Icarus* 47:234–264.

Wiesel, W. 1974. *A Statistical Study of the Kirkwood Gaps*. Ph.D. Dissertation, Harvard Univ., Cambridge, MA.

Wiesel, W. 1982. Saturn's rings: Resonances about an oblate planet. *Icarus* 51:149–154.

Wisdom, J. 1982. The origin of the Kirkwood gaps: A mapping for asteroidal motion near the 3:1 commensurability. *Astron. J.* 87:577–593.

Yoder, C., Colombo, G., Synnott, S., and Yoder, K. 1983. Theory of motion of Saturn's coorbital satellites. *Icarus* 53:431–443.

# DYNAMICS OF NARROW RINGS

STANLEY F. DERMOTT
*Cornell University*

*The ring models described here were developed to account for the dynamical problems posed by the narrow rings of Uranus. Some of these rings are now known to be eccentric, inclined, nonuniform in width, optically thick, and narrow, with very sharp edges. The eccentric rings have common pericenters and large, positive eccentricity gradients. The theory of shepherding satellites successfully accounts for most of these features and can also account for some features of the narrow Saturnian rings, in particular, waves, kinks, and periodic variations in brightness. Outstanding problems include the putative relation between eccentricity and inclination displayed by eight of the nine Uranian rings, and the magnitudes of the tidal torques acting on the shepherding satellites. The horseshoe-orbit model, although viable, probably has more application to the narrow rings from which the Saturnian coorbital satellites formed. The angular momentum flow rate due to particle collisions is a minimum at the Lagrangian equilibrium points $L_4$ and $L_5$, and we can expect accretion to be rapid at these points.*

The Voyager 2 image (Fig. 1) of the Saturnian F Ring showing the two "guardian" satellites, 1980S26 and 1980S27, leaves little doubt that the theory of shepherding satellites proposed by Goldreich and Tremaine (1979*a*) for the Uranian rings is essentially correct. There is no direct evidence that satellites confine the nine Uranian rings, but this must be regarded as very likely. The horseshoe-orbit model of Dermott et al. (1979), postulates that each narrow ring *contains* a small satellite. While viable, this model cannot account for some of the observed features of the Uranian rings. However, I will argue that the model can be applied to the narrow rings from which the coorbital Saturnian satellites presumably were formed. The aim of this chapter

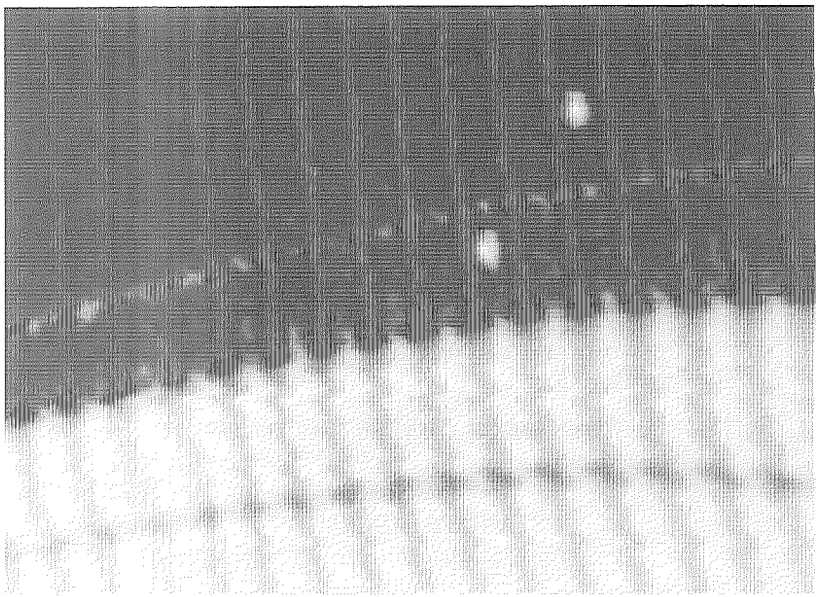

Fig. 1. Image taken by Voyager 2 of Saturn's A Ring, showing the narrow F Ring bracketed by its two shepherding satellites. Because the inner one (1980S27) orbits the planet slightly faster than the outer (1980S26), the satellites lap each other every 25 days. When this picture was taken, the shepherds were $<1800$ km apart; they passed each other $\sim 2$ hr later. Marked azimuthal variations in the brightness of the F Ring are evident. (Image courtesy of JPL/NASA.)

therefore will be to give an account of the dynamical processes involved in both types of ring-satellite gravitational interaction.

In Sec. I, I describe the problems posed by the narrow Uranian and Saturnian rings. The initial outstanding problem was that of particle confinement, and a good portion of this chapter is devoted to that problem alone. In the model of Goldreich and Tremaine (Sec. II), particle confinement is achieved by tidal torques exerted on the ring by small nearby satellites. The torque arises from the second-order change in semimajor axis experienced by each ring particle at each close encounter with the shepherding satellite. However, for the cumulative change in semimajor axis to be finite, the ring particle must lose some orbital energy between consecutive encounters. This loss is achieved either by collisions, which result in eccentricity damping, or by energy transfer to other ring particles through the excitation of spiral density waves. I give a simple derivation of the torque equation and explain why this torque is correctly described as a tidal torque. In Sec. II, I also discuss wave formation in very narrow rings and show how these waves could account for the kinks, braids, and periodic variations in brightness displayed by the Saturnian F Ring.



The linear relation between ring width and orbital radius displayed by the $\epsilon$ Ring of Uranus and some other narrow rings shows that the pericenters of the particle orbits have a common precession rate, and that the pericenters are closely aligned (Sec. III). Such alignment may be maintained by the ring's self-gravitation (Goldreich and Tremaine 1979*a,b*), in which case the ring mass and surface density can be deduced from observable ring parameters. However, it is notable that all the measured eccentricity gradients are close to unity; this prompted Dermott and Murray (1980) to suggest that the rings are close-packed at pericenter and that apse alignment is maintained by particle collisions. This problem has since been complicated by the observation that some Uranian rings have small inclinations, and by a possible relationship between a ring's eccentricity and its inclination (French et al. 1982). Node alignment is easily accommodated by the self-gravitational model (Borderies et al. 1982*a*; Yoder 1983), but at present there is no theory to account for the putative relation between eccentricity and inclination. In Sec. III, I also discuss how recent developments of the shepherding-satellite model of Goldreich and Tremaine account for the existence of rings with very sharp edges.

In the horseshoe-orbit model (Sec. IV), confinement is achieved by the gravitational action of a satellite embedded in the ring; this satellite also acts as a source of ring particles. The dynamics of this problem are of particular interest when the satellite/planet mass ratio, $m/M$, is very small $(m/M)^{\frac{1}{2}} \ll 1$, for only then are the horseshoe-orbit solutions of the equations of motion dominant. I discuss the stability of this type of orbit and the formation of coorbital satellites. A question of interest here is the complete absence of coorbital satellites in the Jovian system, in contrast to their relative abundance around Saturn.

The most important recent review to emphasize the dynamics of narrow rings is by Goldreich and Tremaine (1982). Other reviews include those of Ip (1980*a, b*), Dermott (1981*a*) and Brahic (1982).

## I. PROBLEMS

### A. Observations.

The models described in this chapter were inspired by the discovery of the rings of Uranus (Elliot 1977, 1979), so it is appropriate that I describe these rings first. Here I emphasize only those features which constrain the models; for a more complete description of the Uranian rings see the chapter by Elliot and Nicholson in this book.

All the radii of the nine Uranian rings lie in a comparatively narrow range of radial width $<10{,}000$ km. The innermost ring is 16,000 km above the planet and the outermost ring is 78,000 km lower than the orbit of Miranda. The rings are very narrow and optically thick (optical depths $\tau \lesssim 1$). In fact,

only three of the rings have been fully resolved. These have been found to have nonuniform widths. The width of the $\epsilon$ Ring (the outermost one) increases from 21 km at pericenter to 96 km at apocenter and has a mean normal optical depth $\tau \approx 1$ at its widest point; the optical depth at the narrowest point is too high to be measured reliably. The width of the $\alpha$ Ring increases from 5 km at pericenter to 10 km at apocenter and the corresponding range of $\tau$ is 1.4 to 0.7. The figures for the $\beta$ Ring are similar; the range in width is 5 to 11 km and the corresponding range in $\tau$ is $\sim$1.5 to 0.35. All the other rings except the $\eta$ Ring have widths $< 4$ km (see chapter by Elliot and Nicholson; also Nicholson et al. 1982).

The edges of some of the rings are remarkably sharp; witness the Fresnel diffraction spikes exhibited by, for example, the $\gamma$ Ring. The Voyager 2 photopolarimeter occulation profiles (Lane et al. 1982) have revealed that the outer edge of Saturn's A Ring, located at the 7:6 resonance with the larger coorbital satellite (1980S1), is sharp on a distance scale $<1$ km. The outer edge of Saturn's B Ring, at the 2:1 resonance with Mimas, is comparably sharp. In Sec. III, I discuss the role of resonance in the formation of these sharp edges (Borderies et al. 1982*b*). The Uranian rings are very dark and particulate (gaseous rings [Van Flandern 1979] can be discounted for the reasons given by Fanale et al. [1980], Gradie [1980] and Hunten [1980]). There appears to be very little material between the rings (Matthews et al. 1982).

Most of the resolved rings show some structure. That of the $\epsilon$ Ring has been described as undulating and appears to be stable, i.e., time independent. Near apoapse, the optical depth of the $\alpha$ Ring is a minimum near its center: the so-called "double-dip" structure (see chapter by Elliot and Nicholson). A similar structure is displayed by the narrow ring in Saturn's C Ring at 1.29 Saturn radii ($R_s$) (Sandel et al. 1982) and by the narrow, optically thick spike discovered by the Voyager 2 PPS in Saturn's F Ring (Lane et al. 1982). The Uranian $\eta$ Ring is broad (width $\approx$ 50 km) and diffuse with a sharp, unresolved spike at its inner edge, just inside a region of low optical depth (see Fig. 6 in chapter by Elliot and Nicholson). The $\delta$ Ring also shows a broad section of diffuse material.

That the rings may be eccentric was suggested by Elliot et al. (1977), developed by Lucke (1978), and proved by Nicholson et al. (1978) who discovered the linear relation between the radii and the radial widths of sections of the $\epsilon$ Ring (see Sec. III). All the Uranian rings, with the possible exceptions of the $\eta$ and $\epsilon$ Rings, are now known to be both eccentric and inclined to the equatorial plane of the planet (French et al. 1982). It also appears that all the rings except the $\epsilon$ Ring have $e \approx \sin i$ (to within a factor $<5$), where $e$ is eccentricity and $i$ inclination, and that both $e$ and $i$ increase with decreasing semimajor axis $a$ (see Fig. 14 of Elliot and Nicholson, in this book). If this relation has some physical significance, then the rate of increase of $e$ with decreasing $a$ is so marked that the inner boundary of the ring system



may be that region where $2ae$ would be comparable with the mean ring separation; this would occur at $a \approx 38{,}000$ km.

Most of the structure observed in Saturn's rings is probably due to either diffusion instabilities (Lin and Bodenheimer 1981; Lukkari 1981; Ward 1981) or spiral density waves (Goldreich and Tremaine 1978*b*; Cuzzi et al. 1981). However, in almost every case where clear gaps appear in the rings, eccentric ringlets are found (Smith et al. 1981, 1982; Stone and Miner 1982; Lane et al. 1982). Narrow eccentric rings exist at 1.29 $R_s$ (associated with the Titan apsidal resonance [Porco et al. 1982]), at 1.45 $R_s$, and at 1.95 $R_s$. The latter is just outside the 2:1 Mimas resonance, but appears to be a Keplerian ellipse precessing under the influence of Saturn's oblateness (Smith et al. 1982). In each case, like the eccentric Uranian rings, these rings are widest at apocenter and narrowest at pericenter.

At least two narrow discontinuous rings, or arcs, exist within the Encke Division near 2.21 $R_s$. Two separate rings were seen in the Voyager 1 images, whereas the Voyager 2 images of the gap each show only one ring, but in different images these arcs appear at more than one radial location suggesting that the ring or rings may be discontinuous. Both arcs show large azimuthal variations in brightness on a length scale of 3000 km, and one arc shows kinks or waves tens of km in amplitude (peak to peak) and 1000 km apart (Smith et al. 1982; chapter by Cuzzi et al.).

The strangest narrow ring in the solar system is undoubtedly the F Ring of Saturn discovered by Pioneer 11 (Gehrels et al. 1980). Voyager 1 images of this ring revealed "braids," regions where the ring is split into two separate components (see Fig. 2), clumps, kinks, and large azimuthal variations in brightness (Smith et al. 1981). Braiding was also seen by Voyager 2, but only in one image (Fig. 3) (Smith et al. 1982). The braids or loops have lengths between 7000 and 10,000 km; the initial report of a length of 700 km (Smith et al. 1981) was a mistake (Smith et al. 1982). The spacing of the clumps is similar, but ranges from 5000 to 13,000 km (Smith et al. 1982). These clumps appear fuzzy on most images, but at least one clump is sharply defined and may be a small satellite embedded in the ring (Smith et al. 1982). The widths of the loops shown in the Voyager 1 images are between 30 and 40 km (Smith et al. 1981, 1982).

In the Voyager 2 images, the F Ring appeared 500 km wide and consisted of one bright component and at least four faint components. The Voyager 2 PPS detected a ring of width about 60 km with a sharp, 1 km wide, optically thick ($\tau \approx 1$) component (Lane et al. 1982).

### B. Confinement.

Interparticle collisions, Poynting-Robertson light drag and plasma drag cause an unconstrained narrow ring to gradually spread (Goldreich and Tremaine 1979*a*, 1982). Brahic (1977) has shown that a narrow ring of uniform surface density, mass $m_r$, mean radius $r$ and width $W$ ($<<r$) has an

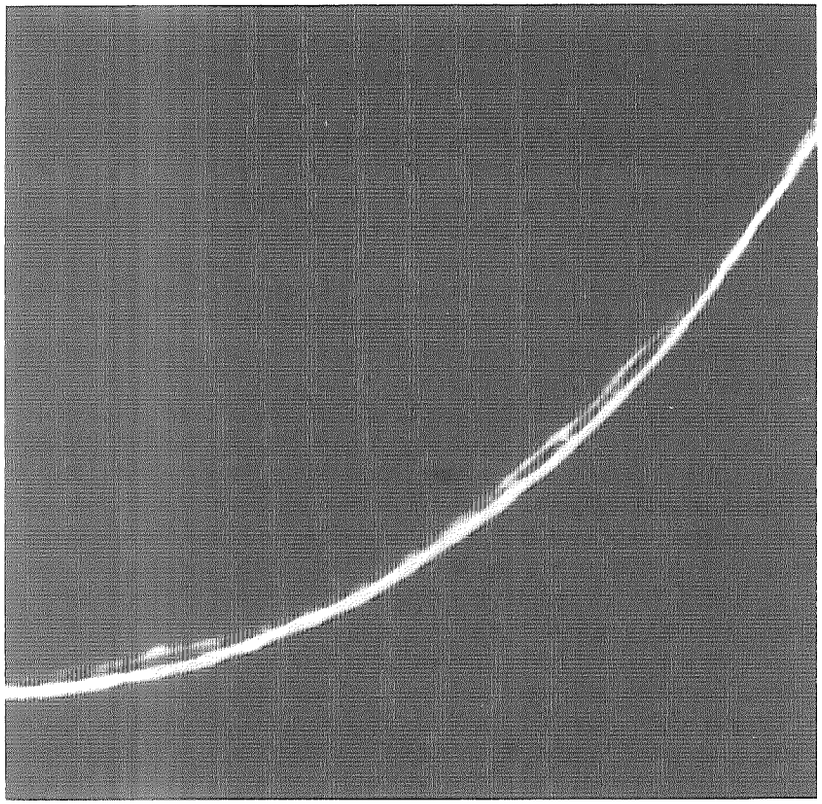

Fig. 2. Three separate components of Saturn's F Ring, seen in a Voyager 1 image. Two prominent bright strands appear twisted and kinked, giving a braided appearance to the ring; the fainter innermost strand largely lacks such nonuniformities. (Image courtesy of JPL/NASA.)

energy $E$ (at fixed angular momentum) that varies with $W$ as

$$E \approx -\frac{GMm_r W^2}{32r^3} + \text{constant}, \tag{1}$$

where $M$ is the mass of the planet and $G$ the gravitational constant. Thus $E$ is a maximum when $W$ is a minimum, and any loss of energy will result in spreading on a timescale $t_d$ given by

$$t_d = W/\dot{W} = -m_r\,\Omega^2 W^2/(16\,\dot{E}) \tag{2}$$

where $\Omega \equiv (GM/r^3)^{\frac{1}{2}}$ is the mean angular velocity of the ring. On the microscopic scale, we can relate $\dot{E}$ to the particle collision frequency $\omega_c$ by



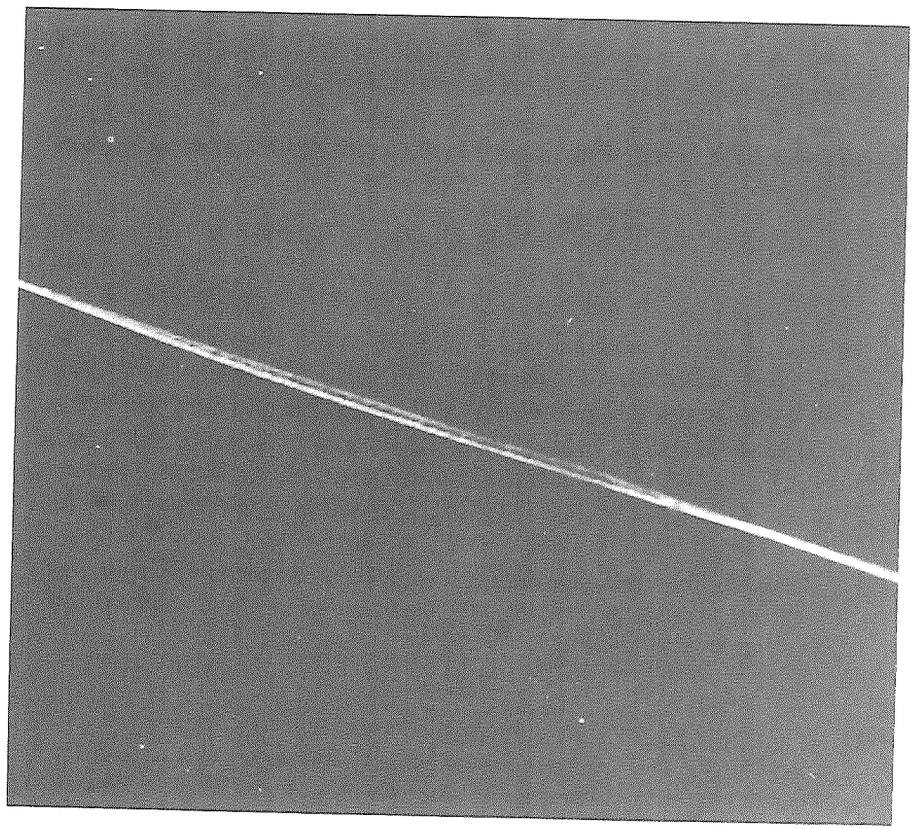

Fig. 3. The only Voyager 2 image of the F Ring that shows braiding. (Image courtesy of JPL/NASA.)

$$\dot{E} \approx -3\mathrm{v}^2 m_r\,\omega_c\,(1-\epsilon^2) \tag{3}$$

where v is the one-dimensional random velocity and $\epsilon$ is the coefficient of restitution of the particles (Goldreich and Tremaine 1982). An alternative approach is to treat the ring as a differentially rotating fluid of density $\rho$ in which a shear stress

$$S \equiv \rho\nu r\,\frac{\mathrm{d}\Omega}{\mathrm{d}r} \tag{4}$$

generates a torque which transfers angular momentum with direction and rate determined by the angular velocity gradient $\mathrm{d}\Omega/\mathrm{d}r$ (Safronov 1969; Lynden-Bell and Pringle 1974). $\dot{E}$ is then the work done by the torque. For effective kinematic viscosity $\nu$ we have

$$\nu = \frac{v^2}{\Omega} \frac{0.46\tau}{1+\tau^2} \tag{5}$$

(Cook and Franklin 1964; Goldreich and Tremaine 1978*a*). Both approaches yield the result that $t_d$ is comparable to the time a particle needs to random walk across the ring (Brahic 1977; Goldreich and Tremaine 1978*a*),

$$t_d \approx \frac{1}{\tau\Omega}\left(\frac{W}{d}\right)^2 \tag{6}$$

where $d$ is the characteristic radius of the particles. For discussion of the meaning of "characteristic" see Hénon (1981, 1983), Goldreich and Tremaine (1982), and the chapter by Weidenschilling et al. For rings located at about 2 planetary radii,

$$t_d \approx \frac{2\times 10^{-4}}{\tau}\left(\frac{W}{d}\right)^2 \text{ yr.} \tag{7}$$

Poynting-Robertson light drag causes the orbit of a particle of density $\rho_r$ and radius $d$, moving in a circular orbit about a planet of mean orbital radius $a_p$, to decay on a time scale

$$t_{\rm pr} \approx \frac{8\rho_r dc^2}{3(L_\odot/4\pi a_p^2) Q_{\rm pr}(5+\cos^2 i)} \tag{8}$$

where $L_\odot$ is the solar luminosity, $c$ is the velocity of light, $i$ is the inclination of the particle orbit relative to the ecliptic and

$$Q_{\rm pr} = Q_{\rm abs} + Q_{\rm sca}(1-\langle\cos\alpha\rangle) \tag{9}$$

where $Q_{\rm abs}$ is the absorption coefficient (1 for a perfect absorber), $Q_{\rm sca}$ is the scattering coefficient, and $\alpha$ is the scattering angle (Burns et al. 1979); see also the chapter by Mignard. The orbits of particles of different sizes will decay at different rates and, despite the effects of collisions which will average out the decay rates, if the surface density of the ring is not radially uniform, then we must expect a narrow ring to broaden on a time scale

$$t_{\rm spread} \approx t_{\rm pr}(W/r) \ . \tag{10}$$

For the Uranian rings

$$t_{\rm spread} \approx 2 \times 10^5 Wd \text{ yr}, \tag{11}$$

where $W$ is in km and $d$ is in cm. Since $t_d$ increases and $t_{\rm spread}$ decreases if $d$ decreases, and vice versa if $d$ increases, it follows that regardless of particle size narrow rings could not remain narrow for more than about $10^7$ yr. Therefore, if the observed narrow rings are not young, then they must be confined (Goldreich and Tremaine 1979*a*).



If a planet has a magnetic field which maintains a corotating magnetosphere, and recent observations of auroral hydrogen Lyman-$\alpha$ emission (Clarke 1982) indicate that this is the case for Uranus as well as Saturn, then absorption of this plasma by the ring particles leads to orbital decay on a timescale

$$t_p \approx \frac{2\,dp_r}{3\,r\rho_p} \frac{\Omega}{(\Omega-\Omega_p)^2} \tag{12}$$

where $\Omega_p$ is the angular velocity of the planet and $\rho_p$ is the plasma density (Burns et al. 1980). Since the planet is the source of the angular momentum, then plasma drag, like tidal drag, acts to push the particles away from the synchronous orbit (see chapter by Grün et al.). For the F Ring of Saturn

$$t_p \approx 3 \times 10^7 d \text{ yr}, \tag{13}$$

where $d$ is in cm. However, since the F Ring partially clears out its flux tubes, the above estimate is a lower limit (Goldreich and Tremaine 1982).

### C. Corotational Resonance.

Shortly after the discovery of the narrow Uranian rings, it was suggested that the observed occultations may have been produced by arcs of particles librating in stable, corotational resonances (Dermott and Gold 1977). The dynamics are illustrated in Fig. 4 (see also Greenberg 1984 and the chapter by Franklin et al.). In a resonance of the type shown, we have

$$(p+q)\lambda' - p\lambda - q\tilde{\omega}' = \phi \tag{14}$$

where $\lambda$ and $\lambda'$ are, respectively, the mean longitudes of a particle and of the perturbing satellite, $\tilde{\omega}'$ is the pericenter of the perturbing satellite's eccentric orbit, and $p$ and $q$ are integers. In the stable configuration $\phi$ librates (i.e. oscillates) about $\pi$; if $q=1$ (first-order resonance), then all conjunctions of the satellite and the particle take place near the apocenter of the satellite's orbit. Thus, the existence of the resonance guarantees that the separation of particle and satellite at conjunction is close to a maximum. (If $q=2$ (second-order resonance), then only every other conjunction takes place near apocenter, and so forth.) Resonances can involve the motions of nodes or even combinations of the motions of nodes and of pericenters, but these more complex cases are not discussed here (see chapters by Franklin et al., and by Shu; also Greenberg 1984).

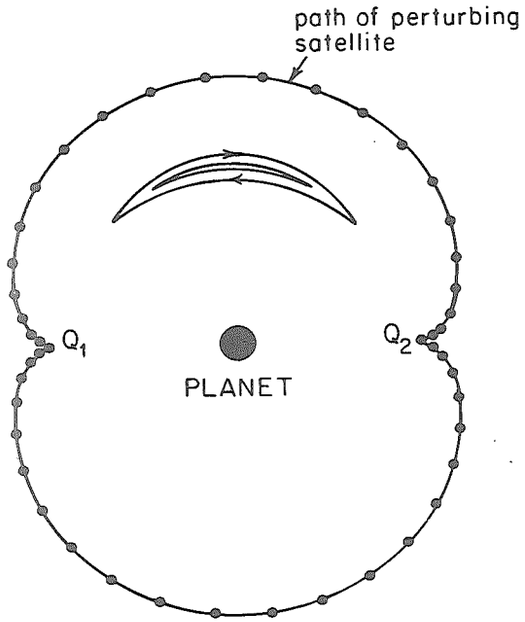


Fig. 4. Libration of particles in a corotation resonance about a longitude which is stationary in a frame corotating with the pattern speed of the perturbing potential. In this frame, the path of the perturbing satellite is closed and stationary. The example shown here is the 3:2 ($\approx n/n'$) resonance. Points marked on the path of the perturbing satellite denote positions at equal time intervals. The motion of the perturbing satellite in this frame is slow near the points marked $Q_1$ and $Q_2$.

Differentiating Eq. (14) with respect to time and rearranging, we obtain

$$\frac{n'-\dot{\tilde{\omega}}'}{n-\dot{\tilde{\omega}}'}=\frac{p}{p+q}\,. \tag{15}$$

Thus, the mean motions relative to the motion of the pericenter are exactly commensurate. It follows that, in a frame rotating with the mean motion $n$ of the particle, the path of the perturbing satellite is closed (see Fig. 4). The gravitational influence of the perturbing satellite on the orbit of the particle can now be modeled by spreading the mass of the satellite along its closed path in such a way that the line density at any one point is proportional to the time spent in that part of the path. In Fig. 4, the positions of the satellite are marked at equal time intervals; thus the spacing of these marks is a measure of the line density. The line density distribution represents the disturbing potential, and we can say that in a corotational resonance the resonant particle corotates with the pattern speed of the disturbing potential. The example shown in the 3:2 resonance ($[p+q]/p=3/2$), for which the line density is a



maximum at the points marked $Q_1$ and $Q_2$. Different values of $p$ and $q$ give rise to different distributions of mass, but in all cases, if the orbital eccentricity of the satellite is not zero, then the line density distribution is not uniform. It is this azimuthal nonuniformity which gives rise to the forces that stabilize the resonance. Consider a particle displaced from the equilibrium point. If the particle is displaced towards the planet, then its mean motion will be greater than the resonant mean motion $n$ and, as shown in Fig. 4, it will drift in the prograde sense. The force on the particle due to the mass distribution at $Q_1$ will then have a greater effect than that at $Q_2$, and will act to increase the angular momentum of the particle. But, since mean motion decreases with increasing angular momentum, the net effect of the force is to reverse the sense of drift. Thus, a displaced particle can librate about a longitude that is fixed in the rotating reference frame. Particles moving in nested librating paths (see Fig. 4) will form a compact arc of particles, that is, a narrow discontinuous ring (Dermott and Gold 1977).

Particle arcs associated with corotational resonances have some interesting properties. Weak external drag forces, such as Poynting-Robertson light drag, do not necessarily destroy their stability; the perturbing satellite can supply the angular momentum removed by the drag force in such a way that the exact resonance is maintained, and the equilibrium longitude in the rotating reference frame is merely displaced (Goldreich 1965). Internal dissipation due to particle collisions still leads to ring spreading, but, since for small displacements the libration period is independent of the libration amplitude, the shear forces and the net angular momentum flow rates due to particle collisions are very much less than in an unconstrained ring of similar proportions (Dermott et al. 1983).

The weakness of this ring model is that for most resonances the arcs are very narrow (Aksnes 1977; Goldreich and Nicholson 1977). The maximum width $W$ of an arc of librating particles is determined by the strength of the average perturbing force and is given by

$$W=8\left(\frac{a|R|}{3GM}\right)^{\frac{1}{2}}a \tag{16}$$

where $a$ is the semimajor axis of the ring particles, and $R$ is the term in the expansion of the disturbing function associated with the resonant argument (Goldreich and Nicholson 1977; Dermott and Murray 1983). For two-body resonances of the type described by Eq. (14),

$$\frac{a|R|}{GM}=\frac{\alpha f(\alpha)m'e'^{q}}{M} \tag{17}$$

where the primed quantities refer to the perturbing satellite and $\alpha = a/a'$.

TABLE I

Arc Widths of Corotational Resonances

| Satellite | $m'/M$ | $e$ | $p+q:p$ | $a$ (Planetary Radii) | $\alpha f(\alpha)$ | $W$ (km) |
|---|---|---|---|---|---|---|
| Mimas | $7\ 10^{-8}$ | 0.0201 | 2:1 | 1.95 | 0.750 | 18 |
| | | | 5:3 | 2.20 | 2.329 | 5 |
| 1980S1 | $8\ 10^{-9}$ | 0.0070 | 5:4 | 2.17 | 3.145 | 8 |
| | | | 6:5 | 2.23 | 3.946 | 9 |
| | | | 7:6 | 2.27 | 4.747 | 10 |
| Miranda | $10^{-6}$ | 0.012 | 4:1 | 1.97 | 0.097 | 0.1 |

Values of $\alpha f(\alpha)$ and $W$ for a few of the corotational resonances in Saturn's rings near Encke's Gap are given in Table I. The arcs associated with these particular resonances are wide and should give rise to observable phenomena. However, the two-body resonances in the region of the Uranian rings are high-order resonances ($q > 3$), so the perturbing forces are weak and the arcs are narrow ($W < 1$ km). Three-body corotational resonances involving two satellites of masses $m_1$ and $m_2$ and a ring particle are also possible, but, since $|R| \propto m_1 m_2/M^2$, these resonances tend to be even weaker (Aksnes 1977; Goldreich and Nicholson 1977).

The corotational resonance model is a viable ring model in that it can account for narrow discontinuous arcs of confined particles which are to some extent stable against the disruptive effects of Poynting-Robertson light drag and interparticle collisions. However, it was soon realized that the model could not account for the widths of the Uranian rings, and other models were sought. We now know that the Uranian rings are not discontinuous arcs, but arcs associated with known satellites should exist in the Saturnian ring system.

## II. SHEPHERDING SATELLITES

### A. Shepherd Dynamics.

The dynamics of the shepherding satellite model of Goldreich and Tremaine (1979*a*) are not easily described in a few lines. The impulse approximation of Lin and Papaloizou (1979), the usual simple approach, has been rejected by Hénon (1983). There is also the problem of explaining the role of dissipation, since an eccentricity damping term is curiously absent from the "standard formula" (Eq. 25) for the torque (Hénon 1983; Greenberg 1983).



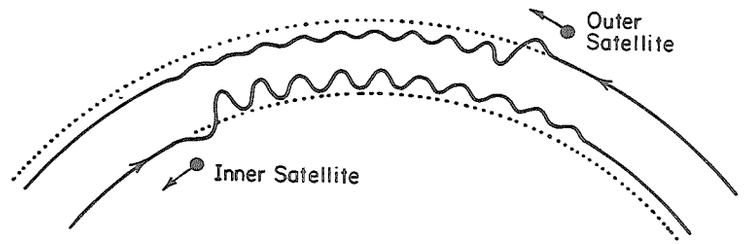


Fig. 5. Schematic diagram showing the action of the shepherding satellites. Arrows on the ring particle paths show the direction of motion of the particles with respect to the perturbing satellite. For clarity I assume here that the outer strand of particles is perturbed only by the outer satellite; in fact both satellites sometimes act on the same particles at the same time, and at all times each satellite acts on all the strands. At conjunction, a satellite changes the eccentricity and the semimajor axis of each ring particle. Eccentricity damping by particle collisions results in a further change in the semimajor axis, but this change is negligible in comparison with that produced by the satellite interaction.

A qualitative description of the mechanism is given in Fig. 5. On encounter with a nearby satellite, a ring particle briefly experiences an attractive force in the direction of the satellite. For a particle initially moving in a circular orbit, this causes the excitation of a small eccentricity $e$ and a change $\delta a$ in its semimajor axis in such a direction that the particle appears to have been repelled by the satellite. The change $\delta h$ in the angular momentum $h$ of the particle is given by

$$2\frac{\delta h}{h} = \frac{\delta a}{a} - e^2 . \tag{18}$$

However, even though we usually have $ea >> \delta a$, $\delta a/a >> e^2$ (see Eq. 21) and $\delta h$ is effectively determined by $\delta a$ alone. But, paradoxically, $\delta a/a$, which is of second order in $m'/M$, can be calculated from $e$, which is of first order in $m'/M$, using the Jacobi integral for the circular restricted three-body problem, or equivalently Tisserand's relation:

$$\frac{a'}{a} + 2\left(\frac{a}{a'}\right)^{\frac{1}{2}}(1-e^2)^{\frac{1}{2}} = C + \mathcal{O}(m'/M) \tag{19}$$

where $C$ is a constant (Goldreich and Tremaine 1982). Substituting $\Delta a = a - a'$ into Eq. (19) and expanding binomially, we obtain (Dermott and Murray 1981*a*)

$$\frac{3}{4}\left(\frac{\Delta a_n}{a'}\right)^2 - e_n^2 \simeq C - 3 \tag{20}$$

where the subscript $n$ refers to values after the $n$th encounter with the perturb-

ing satellite. Thus, an increase in $e$ always produces an increase in the separation $|\Delta a|$ of the semimajor axes of the ring particle and the satellite.

For the configuration shown in Fig. 5, $\delta a = \Delta a_1 - \Delta a_0$, and substitution into Eq. (20) yields

$$\frac{\delta a}{a} = \frac{2}{3}\frac{a}{\Delta a_0}e^2 . \tag{21}$$

$e$ can be estimated from Gauss's form of the perturbation equation:

$$\frac{de}{dt} \simeq \frac{1}{na}(D \sin f + 2T \cos f) \tag{22}$$

where $D$ and $T$ are the radial and tangential forces (per unit mass) on the particle due to the satellite, and $f$ is the particle's true anomaly. If we neglect $T$ and assume that a radial force $Gm'/\Delta a_0^2$ acts for a time $2\Delta a_0/Ua$ (as in the impulse approximation), where $U = 3n\Delta a_0/2a$ is the relative angular velocity of the particle and the satellite, and that during this brief interval ($0.2P$ where $P$ is the orbital period of the particle), the particle is always close to quadrature and $\sin f \simeq 1$, then we obtain

$$e = \frac{4}{3}\frac{m'}{M}\left(\frac{a}{\Delta a_0}\right)^2 \tag{23}$$

(cf. Lin and Papaloizou 1979). A more accurate calculation by Julian and Toomre (1966) shows that the coefficient in this equation is 2.24 rather than 4/3. That our approximation underestimates the coefficient is partly due to neglecting the tangential force. Although the sign of $T$ changes during the encounter, the sign of $\cos f$ also changes and $< T \cos f >$ is actually far from negligible.

To calculate the mean torque $\Gamma$ exerted on the ring, we must now make an assumption about the effects of repeated encounters between a ring particle and a satellite. In Fig. 5 I assume that collisions between the ring particles act to damp the excited eccentricity, and that at the next encounter with the same satellite the particle is again moving in a circular orbit and experiences the same exchange of angular momentum $\delta h$. Since the time between encounters is $2\pi/U$, Eqs. (18), (21) and (23) (with coefficient 2.24 rather than 4/3) yield

$$\Gamma = \dot{h} = \frac{\delta h}{2\pi/U} , \tag{24}$$

$$= 0.399\left(\frac{Gm'}{n\Delta a_0^2}\right)^2 m_r . \tag{25}$$



In this case, a damping factor does not appear in the equation for the torque because it is assumed that between encounters the excited eccentricity is totally damped.

At the other extreme, if the excited eccentricity is completely undamped, then the evolution of $\Delta a$ due to repeated encounters is described by the Jacobi integral, or more approximately by Eq. (20). Using first-order perturbation theory it can be shown that $e$ does not increase indefinitely but merely oscillates about some mean, and it follows from this and Eq. (20) that to second-order in $m'/M$, in accord with Poisson's theorem on the invariability of semimajor axes, $\Delta a$ must also oscillate about some mean and that the torque on average is zero.

Between these two extremes, we must expect the torque to depend on the rate of eccentricity damping. The following argument makes it clear that this is the case. The existence of a torque $\Gamma$ implies that work is performed and that the total mechanical energy $E$ of the system decreases, i.e., is dissipated as heat, at a rate

$$\dot{E} = -U\Gamma . \tag{26}$$

If $\Delta E$ is the energy dissipated in the time $2\pi/U$ between encounters, then

$$\Delta E = 2\pi\Gamma \tag{27}$$

and, from Eqs. (18), (21), and (23), we have

$$\Delta E = \frac{1}{2} m_r (ean)^2 . \tag{28}$$

That is, $\Delta E$ may be thought of as the kinetic energy associated with the radial or eccentric motion of the ring particles. The magnitude of the torque is related to the rate at which this energy is dissipated.

**B. Wave Formation.**

In a frame corotating with the perturbing satellite, all particles initially moving in circular orbits must follow identical paths after encounter. It follows that each satellite generates a standing wave of amplitude $A = ea$ and wavelength

$$\ell = \frac{aU}{n/2\pi} = 3\pi\Delta a_0 \tag{29}$$

(see Fig. 5). In the inertial frame, each particle moves in an independent Keplerian ellipse, but the pericenters of these elliptical orbits and the phases of the particles on the orbits are such that the locus of the particles is a

sinusoidal wave that moves through the ring with the angular velocity of the perturbing satellite (Dermott 1981*b*). For the F Ring of Saturn

$$A = 6 \times 10^{15} (m'/M) (\Delta a_0)^{-2} \text{ km} \tag{30}$$

where $\Delta a_0$ is in km, and

$$\ell = 9.4 \Delta a_0 . \tag{31}$$

Just as the Moon is attracted by the tidal wave that it raises on the Earth, the satellite is attracted by the tidal wave that it raises on the ring, and the calculation of this force gives us another way of estimating the torque $\Gamma$. For heuristic purposes, the ring particles are shown in Fig. 6 as unperturbed ($x=0$) before encounter ($y<0$), and with a displacement

$$x = ea \sin(2\pi y/\ell) \tag{32}$$

after encounter ($y>0$). The torque can easily be shown to be

$$\Gamma = 2.24 \frac{3I}{2\pi} \left( \frac{Gm'}{n\Delta a_0^2} \right)^2 m_r \tag{33}$$

(cf. Eq. 25), where

$$I = \int_0^\infty \frac{(y/\Delta a_0) \sin(2y/3\Delta a_0) \, d(y/\Delta a_0)}{[1 + (y/\Delta a_0)^2]^{\frac{5}{2}}} \approx \frac{1}{6} . \tag{34}$$

Thus, in this approximation the coefficient in Eq. (33) is 0.18 rather than 0.399. This discrepancy is due to my oversimplified representation of the particle path. The wave is only truly sinusoidal when $y$ is large ($>> \ell$). Also, the phase of the wave in Fig. 6 is not an accurate representation of the true phase, but the basic physics is correct. Note that the mean torque is finite only if the wave maintains a constant phase with respect to the satellite. For this reason, a satellite only interacts with its own wave; the waves raised by other satellites have no direct effect, although effects may arise if the eccentricity damping mechanism is nonlinear.

### C. Lindblad Resonance.

In any narrow section of a ring, the perturbations of the ring particle orbits are highly coherent, and, although particle collisions will act to damp the waves, the process may be slow. For this reason, the magnitude of the torque given by Eq. (25) may in some circumstances be an overestimate. If



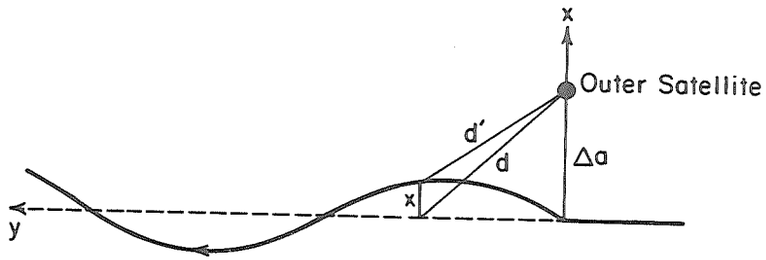


Fig. 6. The tidal torque estimated from the force on the satellite due to the wave. The integral (Eq. 34) is dominated by contributions from those particles with $|y| < \ell/2$. Since $d' < d$, those particles with $y>0$ exert a greater force on the satellite than corresponding unperturbed particles with $y<0$. Thus, the resultant force accelerates the motion of the satellite and retards the motion of the ring particles. The arrow on the wave shows the direction of motion of the ring particles with respect to the outer perturbing satellite.

the waves survive from one encounter to the next, then we must consider the possibility of resonance (see chapter by Franklin et al.). This will occur wherever the local ring circumference is an integral number of wavelengths, that is, wherever

$$2\pi a/\ell = p+1 \tag{35}$$

where $p$ is an integer $\geq 0$. Consecutive perturbations will then be in phase and a wave with amplitude significantly $> A$ may result.

The approximate resonance condition can also be written

$$\frac{n'}{n} \approx \frac{p}{p+q} \text{ or } \frac{p+q}{p} , \tag{36}$$

depending on whether the perturbing satellite is outside or inside the ring, respectively. For a satellite outside the ring ($n' < n$) the exact resonance condition is

$$pn - (p+q) n' + q\dot{\tilde{\omega}} = 0 \tag{37}$$

where $\tilde{\omega}$ is the pericenter of the ring particle orbit. For Lindblad resonance, the order of the resonance $q$ must be unity. (There are also Lindblad resonances with terms in $\tilde{\omega}'$, but those are not discussed here; see Greenberg 1984 and chapters by Franklin et al., and by Shu.) If the particle is locked in resonance and the forced eccentricity is small, then the pericenters of the ring particle orbits are not aligned; rather, $\tilde{\omega}$, $\dot{\tilde{\omega}}$, and the mean longitude or phase of each particle are such that conjunctions of the particle and the satellite always occur at an apse of the particle's orbit. The magnitude of the forced eccentricity, in the absence of damping, is given by

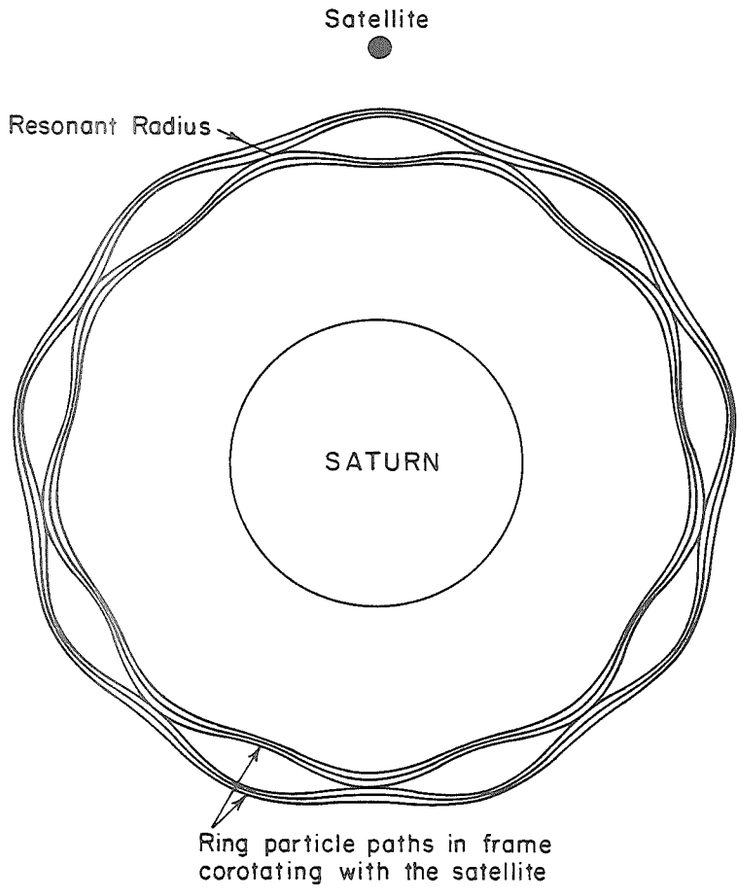


Fig. 7. Ring particle paths in a frame corotating with the perturbing satellite, illustrating the dynamics of Lindblad resonance. Resonant gravitational interactions at radii in the ring where the ratio of the satellite and ring particle mean motions are close to $p/(p+1)$, where $p$ is an integer, generate a system of waves which are stationary in the rotating frame. The waves on opposite sides of the exact resonance have a phase difference of 180°; the resultant wave pattern consists of $p+1$ equally spaced loops. The variations of surface density associated with this pattern can act on the other ring particles to excite a spiral density wave (see Fig. 11). (Figure copyright of *Nature*, MacMillan Journals Ltd.)



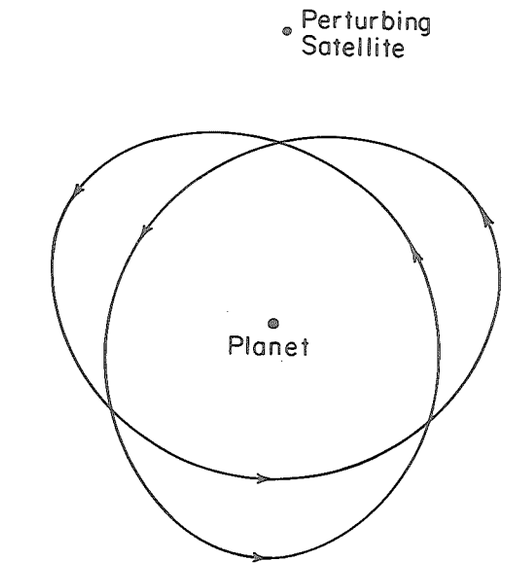


Fig. 8. Path of a particle in a reference frame rotating with the perturbing satellite. The particle is trapped in a 3:1 resonance for which $(p+q)n'-pn-q\tilde{\omega}=0$, $p=1$, and $q=2$. In this frame, all paths for which $q\neq 1$ are self-intersecting. Thus, in a densely populated ring of particles, Lindblad resonances for which $q\neq 1$ cannot be established.

$$e = \left| \frac{1}{2} \frac{(m'/M) f(p) n}{(p+1) n' - pn} \right| \tag{38}$$

(Greenberg 1973). Thus $e$ increases markedly as the exact resonance is approached. At the exact resonance, the phase of the response changes by 180°. Similar behavior is observed in any driven harmonic oscillator. For particles outside the exact resonance, conjunction always occurs at apocenter, whereas for particles inside the exact resonance, conjunction always occurs at pericenter. Thus, the satellite excites a wave pattern of $p+1$ equally spaced loops which corotate with the perturbing satellite (see Fig. 7).

The particle path pattern shown in Fig. 7 is one of streamline flow for which interparticle collisions are a minimum. Such nonintersecting nested paths are possible only if $q=1$ and every conjunction takes place at the same point in the orbit. If $q>1$, then, no matter how small the forced eccentricity, each particle path always intersects itself (see Fig. 8). Obviously, in a densely populated ring of particles, resonant orbits that intersect can neither be established nor maintained.

Even if $q=1$, then, because of the phase change at exact resonance, orbits close enough to exact resonance can still intersect. In Fig. 7, these orbits have been eliminated. The edges of the empty loops are then defined by those orbits

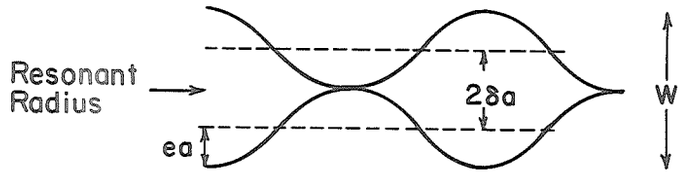


Fig. 9. Particle paths displaced $\delta a(=W/4)$ from exact resonance. Since $ea = \delta a$ and $e = 0.546(m/M)/(\delta a/a)$, we have $W = 2.96\,(m/M)^{\frac{1}{2}}a$.

that are displaced from exact resonance by a distance $\delta a$, such that the resultant forced eccentricity is $\delta a/a$ (see Fig. 9). If $p$ is large, then

$$e = 0.546\,\frac{(m'/M)}{\delta a/a} \tag{39}$$

and $e$ is independent of $p$. Hence, since $ea = \delta a$,

$$0.546\,\frac{(m'/M)}{\delta a/a^2} = \delta a \tag{40}$$

and

$$W = 4\delta a = 2.96\,(m'/M)^{\frac{1}{2}}a. \tag{41}$$

Thus, $W$ is approximately the same for all first-order resonances. Approximate values of these loop widths for Lindblad resonances in Saturn's rings are given in Table II. If $ea = \delta a$, then

$$\frac{\mathrm{d}(ea)}{\mathrm{d}|\delta a|} = -1 \tag{42}$$

and where the loop width is a maximum the streamlines converge on common points. This occurs at apocenter or pericenter, depending on whether the particle orbits are outside or inside exact resonance. The finite size of the ring particles would prevent such close packing of the particles from occurring, and thus the above value for $W$ should be regarded as an underestimate.

The particle path pattern shown in Fig. 7 represents the undamped configuration. The lag angle between the equilibrium, or steady-state, tide and the tide-raising satellite is zero and there is no torque. Any dissipation of the energy stored in the tidal wave due to interparticle collisions results in a lag in the tidal response of the ring. The resultant torque is proportional to the magnitude of that lag. Figure 10 is a schematic representation of the configuration at the outer edge of the Saturnian B Ring, which is just inside the 2:1 resonance with Mimas.



TABLE II

Loop Widths of Lindblad Resonances

| Satellite | m'/M | $W^a$ (km) |
|---|---|---|
| Mimas | $7 \times 10^{-8}$ | 94 |
| 1980S1 | $8 \times 10^{-9}$ | 32 |
| 1980S3 | $10^{-9}$ | 11 |
| 1980S26 | $6 \times 10^{-10}$ | 9 |
| 1980S27 | $10^{-9}$ | 11 |
| 1980S28 | $2 \times 10^{-11}$ | 2 |

[a]We assume that $p$ is large and that $a \approx 2$ planetary radii.

### D. Spiral Density Waves.

If a ring has sufficiently high surface density, then the azimuthal variation of the gravitational potential associated with the $p+1$ loops at a Lindblad resonance can act on the orbits of the other ring particles, to generate a spiral density wave with $p+1$ arms. The theory of this important ring phenomenon has been described in great detail by Goldreich and Tremaine (1978*b*,*c*, 1979*c*, 1980, 1981, 1982) and is reviewed in the chapter by Shu. Here, I content myself with a few qualitative remarks.

Outside the region of exact resonance, the particle paths in a frame corotating with the perturbing satellite are closed and contain the same number of waves. However, each closed path is displaced azimuthally with respect to its neighbor, and it follows from geometrical considerations that a spiral density wave must result (see Figs. 11 and 12). The whole pattern is stationary in the corotating reference frame. Thus, the gravitational potential associated with the spiral arms acts on the ring particles with the same frequency as the disturbing potential, and the pattern is self-enhancing.

The magnitude of the torque that now arises from the force between the satellite and the spiral arms is still determined by the rate of energy dissipation, but this energy is now dissipated at locations well-removed from the exact resonance. This process has been well described by Harris and Ward (1982) who compare the spiral density waves with "water waves [that] propagate away and leave the site of the original disturbance calm . . . ready for the next impulse." Consistent with this view, detailed calculations by Goldreich and Tremaine (1978*b*,*c*, 1979*c*) show that the magnitude of the torque is given by Eq. (25), that is, by the formula for waves in very narrow rings in which the wave energy is completely dissipated between impluses.

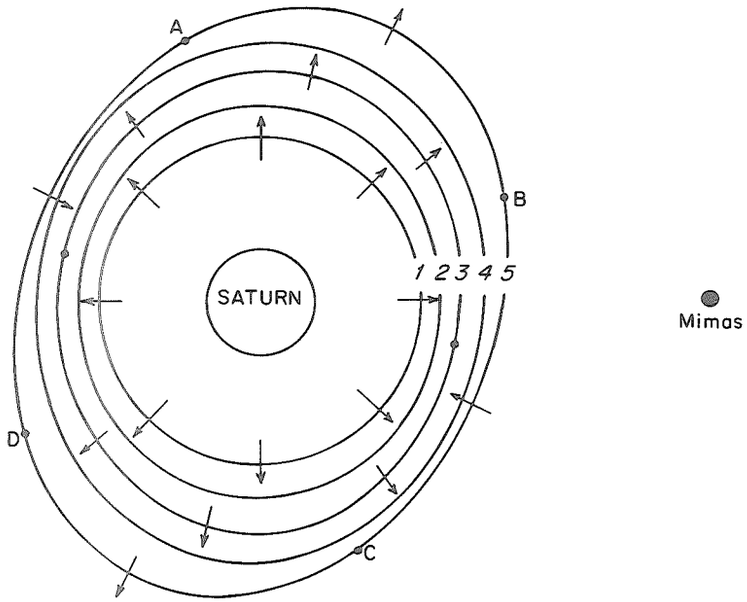


Fig. 10. Particle paths (streamlines) near the 2:1 Lindblad resonance associated with Mimas (located at the outer edge of the Saturnian B Ring). The radial arrows show the direction of angular momentum flow, determined by the local angular velocity gradient. Streamline #3 is critical, having two azimuthal positions (marked with dots) where the angular velocity gradient is zero. Streamline #4 has a limited azimuthal domain in which angular momentum flows inward. For streamline #5, the outward angular momentum flow between A and B and between C and D is exactly balanced by the inward flow between B and C and between D and A, and the net flow across the streamline is zero. According to Borderies et al. (1982*b*), this streamline marks the ring boundary; they have shown that such boundaries can be remarkably sharp. (Figure by P. Goldreich, personal communication.)

For an inner Lindblad resonance, for which (according to Eq. 37) the perturbing satellite is outside the ring and $n/n' \approx (p+1)/p$, the spiral density wave is only present outside the resonance and the torque on the ring is negative. The density wave carries negative energy and angular momentum and propagates towards the satellites. This wave is damped by particle collisions, and those particles involved in the damping lose energy and angular momentum and move inwards towards the planet and away from the perturbing satellite. Consequently, just outside the exact resonance a broad gap may open up (Goldreich and Tremaine 1978*b*, 1982). Gaps and density waves associated with inner Lindblad resonances have been observed in Saturn's rings (Cuzzi et al. 1981). For an outer Lindblad resonance, for which the perturbing satellite is inside the ring and $n/n' \approx p/(p+1)$, the torque on the ring is positive and damping of the density waves causes the particles to move away from the planet and away from the perturbing satellite. In both cases, the perturbing satellite acts to repel the ring particles.



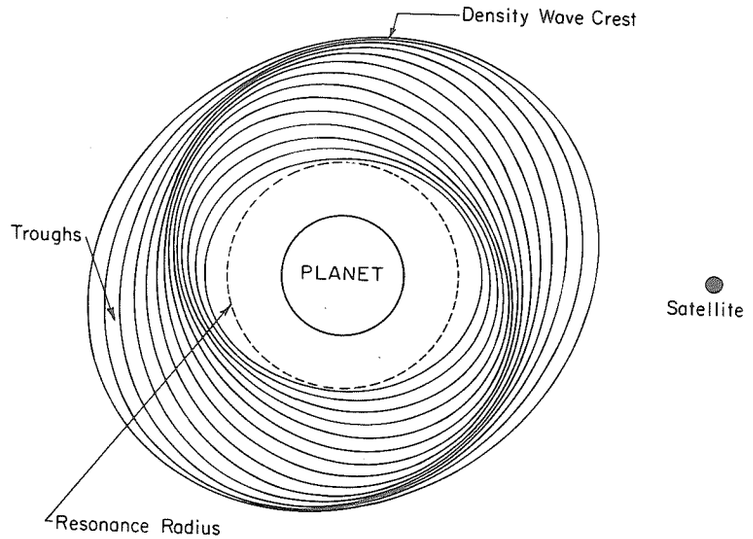


Fig. 11. Schematic diagram of the particle path pattern and the associated trailing spiral density wave generated by the $p=1$ Lindblad resonance. The pattern is stationary in a frame co-rotating with the perturbing satellite.

Ring particles trapped in a corotational resonance form a compact arc of particles (see Fig. 4), and the azimuthal variation of the gravitational potential associated with this arc can also act on the other ring particles to generate a spiral density wave (Goldreich and Tremaine 1979*c*, 1982). Unlike Lindblad resonances, corotational resonances are not confined to first-order ($q=1$) resonances, so the number of possible resonant locations in a ring can be large. However, the width of a corotational arc is less than the width of a Lindblad loop by a factor $\sim e^{|q|/2}$ (see Eqs. 16, 17, and 41) and, since the eccentricities of satellites in the solar system tend to be small, the gravitational influence of a corotational resonance tends to be less than that of a Lindblad resonance.

### E. Goldreich-Tremaine Model.

If a wide, diffuse ring is bounded by two satellites, then the repulsive action of the satellites will reduce the ring width until the confining torques just counteract the tendency for the ring to spread (Goldreich and Tremaine 1979*a*). (This shepherding action will not occur if the motion of the ring particles is retrograde with respect to that of the satellites. In that case, the two torques would act on the ring in the same sense and the space between the satellites would be swept clear of particles.)

In equilibrium, the net external torque on the ring is zero. Hence, from Eq. (25)

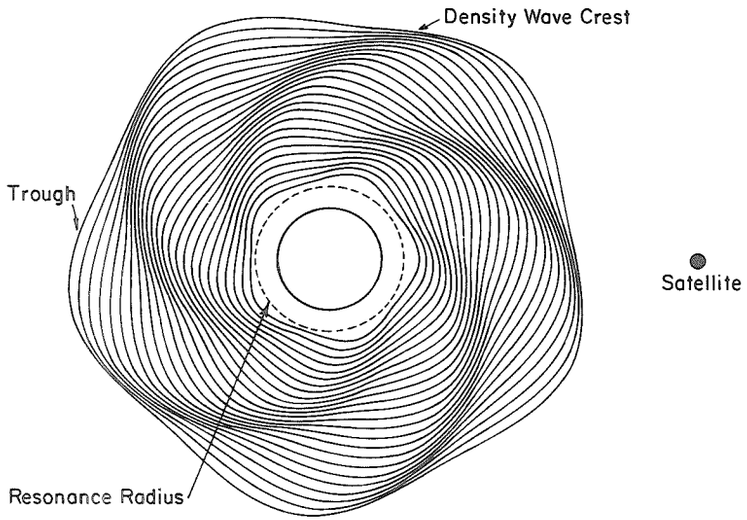


Fig. 12. Schematic diagram of the particle path pattern and the associated trailing spiral density wave generated by the $p=4$ Lindblad resonance. If the ratio of the resonant mean motions is $p/(p+1)$, then $p+1$ spiral arms are generated.

$$\frac{m_{\text{out}}}{\Delta a_{\text{out}}^2} = \frac{m_{\text{in}}}{\Delta a_{\text{in}}^2} \tag{43}$$

where the subscripts 'out' and 'in' refer to the outer and inner satellites respectively. It follows from Eq. (23) that the amplitudes of the two waves raised on the ring are equal, although their wavelengths may be quite different.

Collisions between the ring particles generate a torque

$$2\pi a^3 \sigma \nu \left|\frac{\mathrm{d}\Omega}{\mathrm{d}a}\right| = 3\pi a^2 \sigma \nu n \tag{44}$$

where $\sigma$ is the surface density of the ring. This is the magnitude of the torque that must be applied to the ring to maintain an equilibrium width $W$. The excess torque on each half of the ring due to variations of satellite torques across the ring is of magnitude

$$W < \Delta a^{-1} > |\Gamma| \tag{45}$$

where $|\Gamma|$ is the magnitude of the total torque exerted on the ring by each satellite. Equating Eqs. (44) and (45), and assuming for convenience that $\Delta a_{\text{out}} = \Delta a_{\text{in}} = \Delta a$ and that $\nu \approx n d^2 \tau$, we obtain



$$W = \left(\frac{15\tau}{4}\right)^{\frac{1}{2}} \frac{M}{m}\left(\frac{\Delta a}{a}\right)^{\frac{3}{2}} d \tag{46}$$

where $d$ is the "characteristic" size of the ring particles (Goldreich and Tremaine 1979*a*; see also discussion in chapter by Weidenschilling et al.). Plausible shepherd satellites, for example with $m/M \sim 10^{-10}$ and $\Delta a \sim 500$ km, would give the observed width for the Uranian rings, assuming cm-sized particles. However, the observed width of Saturn's F Ring is ~500 times that given by Eq. (46). Perhaps the problem is that the torque formulae do not strictly apply when the orbits are eccentric. Showalter and Burns (1982) argue that the F Ring particles are appreciably "stirred" at each close encounter with the shepherding satellites and that this could account for the excessive width of the ring.

The torque $\Gamma$ exerted by the ring on each satellite pushes the satellites away from the ring at rates given by

$$\Gamma = h = \frac{1}{2} mna\dot{a} \ . \tag{47}$$

The timescale for the rate of change of $\Delta a$

$$T_{\text{sep}} = \frac{\Delta a}{\dot{a}} = \frac{5}{4} \frac{M^2}{mm_r}\left(\frac{\Delta a}{a}\right)^5 n^{-1} \tag{48}$$

can be used to place bounds on the surface densities of the rings. Using $\sigma = \tau \rho_r d$ and Eq. (46), we can eliminate $mm_r/M^2$ from Eq. (48) to obtain

$$T_{\text{sep}} = 3 \times 10^{14} \tau^{\frac{1}{2}} \left(\frac{\rho_r}{\sigma}\right)\left(\frac{\Delta a}{a}\right)^{\frac{3}{2}} \text{yr} \tag{49}$$

where $\rho_r$ and $\sigma$ are given in cgs units. If we demand that $T_{\text{sep}} > 5 \times 10^9$ yr, then, with cgs units,

$$\sigma < 200 \tau^{\frac{1}{4}} \rho_r^{\frac{1}{2}} (\Delta a/a)^{\frac{5}{4}} . \tag{50}$$

Thus, for the Uranian rings we must have $\sigma < 1$ g cm$^{-2}$, a value which in itself is not objectionable. However, Goldreich and Tremaine (1979*a*,*b*) consider that the apse alignment of the $\epsilon$ Ring is maintained by self-gravitation (see Sec. III), in which case $\sigma \approx 25$g cm$^{-2}$. If $\Delta a/a \approx 10^{-2}$ (and in this argument $\Delta a$ should be regarded as the smaller of $\Delta a_{\text{out}}$ and $\Delta a_{\text{in}}$), then their value for $\sigma$ yields $T_{\text{sep}} \approx 10^7$ yr. If this were the case, we would have to conclude that the $\epsilon$ Ring is very young.

The easiest way out of this dilemma is to allow that $\sigma$ is $<1$ g cm$^{-2}$ and that apse alignment is not maintained by self-gravitation (Dermott and Murray

1980); this is discussed further in Sec. III. Goldreich and Tremaine (1979*a*,*b*) suggest that the guardian satellites may be trapped in corotational resonances with the known Uranian satellites. Since the torque exerted by the ring would have to increase the angular momentum of all the satellites involved in the resonance, $T_{sep}$ would be larger by a factor $\gtrsim m^*/m$, where $m^*$ is the sum of the masses of the resonant satellites. However, most of the possible resonances in the vicinity of the rings are three-body resonances for which

$$\dot{\phi} = qn - (p+q)n_B + pn_A \tag{51}$$

where the subscripts $B$ and $A$ denote the inner and outer satellites respectively (Dermott and Gold 1977; Goldreich and Nicholson 1977; Freedman et al. 1983). I find that these resonances may be too weak to trap the satellites.

The equation of motion of the resonant argument $\phi$ is

$$\ddot{\phi} = -\omega^2 \sin\phi + q\dot{n}_{\text{drag}} \tag{52}$$

where $\dot{n}_{\text{drag}}$ is the rate of change of the mean motion of the guardian satellite due to the ring torque:

$$\frac{n}{\dot{n}_{\text{drag}}} = \frac{a}{\Delta a} T_{\text{sep}} \,. \tag{53}$$

The libration frequency $\omega$ is related to the width $W$ of the corotation arc (see Eq. (16) by

$$\frac{\omega}{n} = \frac{3W}{8a} = \left(\frac{3a|R|}{GM}\right)^{\frac{1}{2}} \,. \tag{54}$$

For stability, the sign of $\ddot{\phi}$ must reverse (Goldreich 1965), hence

$$|q\dot{n}_{\text{drag}}| < \omega^2 \,. \tag{55}$$

For the guardian satellites of the Uranian rings, we need

$$T_{\text{sep}} > 5 \times 10^{-9} q \left(\frac{GM}{\Delta a|R|}\right) \text{ yr.} \tag{56}$$

If we allow that $\sigma \approx 1$ g cm$^{-2}$, then for resonant trapping we need $a|R|/GM > 10^{-16}$; there are indeed many 3-body resonances that satisfy this requirement (Goldreich and Nicholson 1977). However, if $\sigma \approx 25$ g cm$^{-2}$, as is perhaps the case for the $\epsilon$ Ring, then $T_{\text{sep}} \approx 10^7$ yr and for resonant trapping we need $a|R|/GM > 10^{13}$. It so happens that there are two, and only two, resonances close to the $\epsilon$ Ring that satisfy this requirement. The $p = 7$ Miranda-Ariel resonance has a strength $\approx 2 \times 10^{-13}$ and the Miranda 4:1 resonances have strengths $\approx 10^{-11}$ ($e \sin^2\frac{1}{2} i$ term) and $\approx 6 \times 10^{-13}$ ($e^3$ term). However, these resonances have semimajor axes of 50887 km, 51470 km, and 51520 km respectively (data and formulae from Freedman et al. 1983). Thus, the Miranda-Ariel resonance lies $\approx 100$ km outside the pericenter of the $\epsilon$ Ring at 50782 km, and the Miranda 4:1 resonances lie $\sim 100$ km inside the apocenter at 51595 km. Unless the pericenters of the satellites and the ring orbits are permanently aligned (and this possibility is easily dismissed), these resonances cannot be the locations of the guardian satellites.



I conclude that, unless resonances involving unseen satellites that orbit between the rings and Miranda and have masses $> 10^{-8} M$ anchor the guardian satellites, we must have $\sigma \sim 1$ g cm$^{-2}$, and that the apse alignment of the $\epsilon$ Ring is not maintained by self-gravitation. But there is another possibility: Eq. (25) may greatly overestimate the magnitude of the ring torque. That the actual torques are probably much less than those given by Eq. (25) is suggested by the observation (Smith et al. 1981, 1982) that comparatively massive satellites exist close to the Saturnian A Ring. Goldreich and Tremaine (1982) estimate that

$$T_{\text{sep}} = 1.5 \times 10^{-6} \sigma^{-1} R_s^{-3} \Delta a^4 \text{ yr} \tag{57}$$

where $R_s$ is the satellite radius in cm; $\Delta a$ is now the separation in cm of the satellite from the outer edge of the A Ring, and $\sigma$ is in g cm$^{-2}$. $T_{\text{sep}}$ for 1980S1 and 1980S27 may be as small as $7 \times 10^7$ and $6 \times 10^5$ yr, respectively. The orbits of these satellites are well determined, and they are not stabilized by any known resonance (Goldreich and Tremaine 1982). In the case of 1980S27, if we require $T_{\text{sep}} > 5 \times 10^9$ yr, then $< 10^{-4}$ of the energy associated with the excited eccentricities must be dissipated between encounters. If resonances in the A Ring associated with this satellite are strong enough to open gaps, then $T_{\text{sep}}$ may be larger, but only by a factor $\approx 4$ (Goldreich and Tremaine 1982). Perhaps we should consider the possibility that the rings are young.

### F. Kinks, Braids and Eccentric Rings.

The theory that I have described so far is appropriate for near-circular satellite and ring orbits. It may be applicable to some of the Uranian rings, but for eccentric rings, particularly the Saturnian F Ring, modifications are necessary.

All aspects of the F Ring appear somewhat extreme. The amplitudes $A$ of the waves on the ring are $\approx 6(1000 \text{ km}/\Delta a)^2$ km (see Eq. 30) and thus are comparable with the 30 km width of the main ring. For the Uranian rings, with plausible values $m/M \sim 10^{-10}$ and $\Delta a \sim 500$ km, the wave amplitudes are probably very much less than the ring widths.

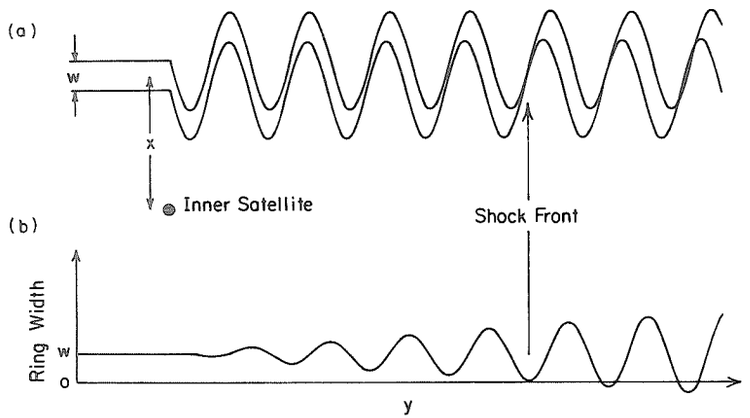


Fig. 13. (a) Wave pattern for a satellite-generated wave of length $3\pi\Delta a$, where $\Delta a$ is the mean distance of the satellite from the ring particles. There is a small variation in wavelength across a ring of finite width. The resultant particle path pattern could lead to the formation of shock fronts and, if the ring contains gaps, loops. This could account for some of the features seen in the Saturnian F Ring. (b) Radial variation of ring width associated with the wave pattern shown in (a).

For a ring of finite width, there is a variation of wavelength across the ring and this can lead to the formation of shocks (see Fig. 13). The shock front will form at a distance

$$y = \frac{3\Delta a^2}{2A} \tag{58}$$

from the perturbing satellite. For $y < 2\pi a$, we require

$$\Delta a < 300 \left(\frac{m/M}{10^{-10}}\right)^{\frac{1}{4}} \text{ km} \tag{59}$$

for the Uranian rings, and

$$\Delta a < 1400 \left(\frac{m/M}{10^{-9}}\right)^{\frac{1}{4}} \text{ km} \tag{60}$$

for the F Ring. Thus, in both cases shocks may form between encounters with the perturbing satellites. The shocks will have radial widths $< A$. For the Uranian rings this may be very small ($<0.1$ km), whereas for the F Ring the radial width of the shocked region could be far from negligible.



Shock fronts are likely sites for the formation of temporary particle clumps, thus I would expect these to have a mean azimuthal separation of one wavelength $\ell$. These shocks and the associated variations of ring width (see Fig. 13) may also contribute to the marked periodic variations in brightness observed in the F Ring and in narrow rings in Encke's gap (Gehrels et al. 1980; Smith et al. 1981, 1982).

The lines drawn in Fig. 13 represent the boundaries of a narrow ring, but they could equally well represent the boundaries of a narrow gap within a ring. In that case, near the shock the gap would degenerate into a series of loops or braids of width $2W$ and length $\ell$, where $W$ is the unperturbed width of the gap. The width of the loops could not exceed $4A$ ($\approx$ 24 km for the F Ring). The gap would be expunged at the shock and thus would have to be regenerated by some agency. A natural suggestion is that small satellites (or large particles) exist in the ring.

The width of the Lindblad loops is

$$W = 1.5 \left(\frac{m/M}{10^{-9}}\right)^{\frac{1}{2}} \tag{61}$$

for the Uranian rings, and

$$W = 13 \left(\frac{m/M}{10^{-9}}\right)^{\frac{1}{2}} \tag{62}$$

for the F Ring. Thus, we could only expect to observe these loops in the F Ring. It was in fact suggested that these loops could account for the braided appearance of the ring (Dermott 1981*b*). However, first-order resonances are separated by a distance

$$s = \frac{3\Delta a^2}{2a} . \tag{63}$$

For the F Ring $s = 7$ km, which is $<< W$. Thus, even if the F Ring were circular the resonant configuration could not be established. For the Uranian rings, assuming $\Delta a \sim 500$ km, $s$ is large enough that the resonances are probably well separated. Borderies et al. (1982*b*) consider that Lindblad resonances define the edge of each narrow ring. This is certainly possible, but for some of the narrow rings the interior of the ring may be free of resonances. Perhaps $s$ defines the minimum width of a sharp-edged ring.

If a ring is appreciably eccentric, then there is no direct application of our discussion of corotational and Lindblad resonance; the only resonance that can exist is an "eccentric" resonance (Goldreich and Tremaine 1981). However, the perturbations can be divided into corotational terms that perturb the mean longitude and Lindblad terms that perturb the eccentricity. Both terms

act to change the ring eccentricity $e_r$. If $e_r << \Delta a/a$, then the resultant time scale $(e_r/\dot{e}_r)$ is

$$T_e = \frac{2}{cn}\left(\frac{M}{m_s}\right)^2 \left(\frac{\Delta a}{a}\right)^5 \tag{64}$$

where the subscript $s$ refers to the guardian satellite (Goldreich and Tremaine 1982). Using Eq. (46) for the ring width $W$ and $\sigma = \tau \rho_r d$ to eliminate $m_s/M$ and $\Delta a/a$, we obtain

$$T_e = 8 \times 10^{-5}\,(\tau/c)\,(W\rho_r/\sigma)^2 \text{ yr} \tag{65}$$

for the Uranian rings, where quantities on the right are given in cgs units. If no gaps are present in the ring, then the corotation terms dominate, $c = -0.148$, and the eccentricity damps. If gaps open at the first-order resonances in the ring, then the Lindblad terms dominate, $c = +1.52$, and the eccentricity grows (Goldreich and Tremaine 1981, 1982). Both timescales are uncomfortably short. We now know that only the $\eta$ Ring appears to be truly circular (French et al. 1982).

The perturbation of a narrow, eccentric ring by a nearby satellite has been studied numerically by Showalter and Burns (1982). They do not take account of interparticle collisions which, particularly in the case of the F Ring, can have a major influence on the particle flow patterns even on timescales as short as the period between encounters. Nevertheless, their methods are well suited for studying the dynamics of encounter, and they have revealed a number of interesting phenomena.

Their satellite-ring configuration is shown in Fig. 14. Only the range of variation of the ring-satellite separation is significant. If the eccentricities are small, then for a given value of this range the separate eccentricities and orientations of the satellite and ring orbits do not matter. The encounter dynamics can be accurately modeled by the simplest configuration, that of a circular ring and a nearby satellite in an eccentric orbit (Showalter and Burns 1982).

There are large, qualitative differences between this case and that of a satellite in a circular orbit. At encounter, there is now a large (first-order in $m/M$) change $\delta a$ in the semimajor axis of the ring particle orbit. For all encounter phases, we estimate that

$$|\delta a| \approx \frac{4}{3}\, a^2 e_s \left|\frac{\delta e}{\Delta a}\right| + 0(m/M)^2 \tag{66}$$

where $\delta e$ is the forced eccentricity still given by Eq. 23 and $e_s$ is the eccentricity of the satellite orbit. However, the actual magnitude and the sign of $\delta a$ vary systematically with the phase of the encounter. The change in sign of



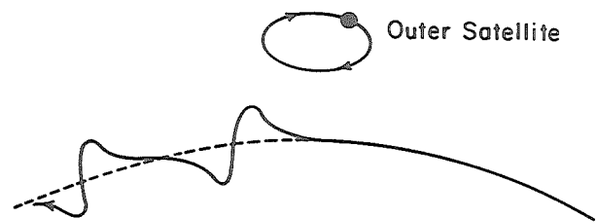


Fig. 14. Wave pattern for a wave, also of length $3\pi\Delta a$, where $\Delta a$ is mean distance of the satellite from the ring, generated by a satellite in an eccentric orbit. This wave is not sinusoidal. In a frame rotating with the mean motion of the perturbing satellite, the path of the satellite is an ellipse with semimajor and semiminor axes $2ae$ and $ae$, respectively.

$\delta a$ is particularly important, since it follows that there is a tendency for gap formation, or at least appreciable azimuthal variations in the particle number density on a scale of one wavelength $\ell$. These variations could be largely responsible for the marked variations in brightness observed in the F Ring, although as I have discussed there could be other contributing factors.

The long-term variations of the eccentricities of narrow rings have been studied by Borderies et al. (1983*a*). In their model, both the ring and the nearby satellite are replaced by one dimensional elliptical wires of line densities $m_r/2\pi a$ and $m_s/2\pi a$, respectively. The radial force between these wires determines the variation of the eccentricity and apse precession rate $\dot{\tilde{\omega}}_r$ of the ring (see Sec. III). The relative influence of the satellite and the quadrupole moment of the planet $J_2$ on $\dot{\tilde{\omega}}_r$ is determined by the ratio

$$\Gamma_e = \frac{21\pi}{2}\,\frac{M}{m_s} J_2 \left(\frac{B}{a}\right)^2 \left(\frac{\Delta a}{a}\right)^3 \tag{67}$$

where $B$ is the radius of the planet. For the Uranian rings, we can again use Eq. (46) to obtain

$$\Gamma_e = \frac{1}{4}\,\tau^{\frac{1}{2}}\,(W\rho_r/\sigma)\,(\Delta a/a)^{\frac{1}{2}}\,. \tag{68}$$

Thus, for these rings, $\Gamma_e >> 1$ and the influence of $J_2$ is dominant. However, for the inner guardian satellite of the F Ring, $\Gamma_e = 16.8$ and there are small but appreciable variations in both $\dot{\tilde{\omega}}_r$ and $e_r$ on a timescale of 18 yr (Borderies et al. 1983*a*).

The configuration of the F Ring and the inner guardian, 1980S27, at the time of the Voyager 2 encounter is shown in Fig. 15. The distance of closest approach was then $\approx$ 483 km. The corresponding radial separation $\Delta r$ of the apocenter and pericenter distances was $+134 \pm 142$ km, and the separation $\Delta a$ of the semimajor axes was $832 \pm 30$ km (Synott et al. 1983). 1980S27 has

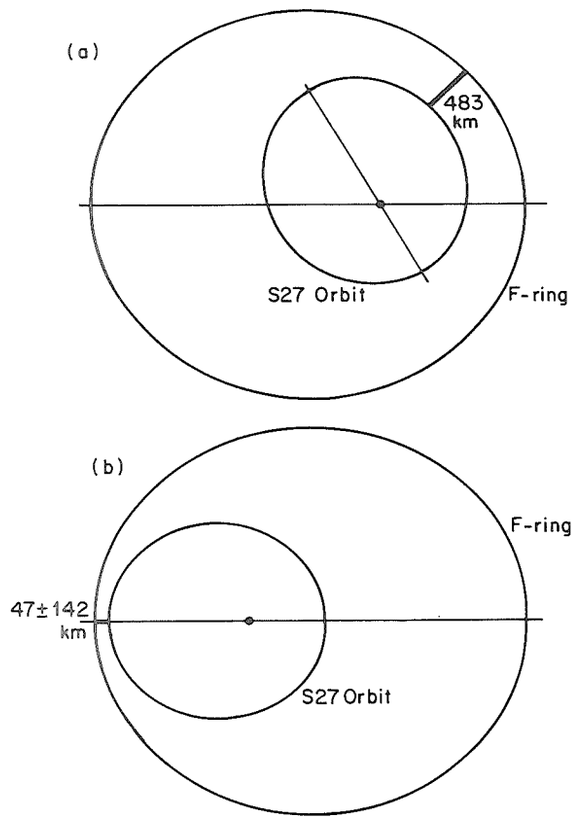


Fig. 15. (a) Configuration of the Saturnian F Ring and inner shepherding satellite (1980S27) orbits, at the time of Voyager 2 encounter. (b) The configuration expected in 1993.

a long semiaxis of 70 km (Smith et al. 1982). Thus, even if the orbital elements were to remain constant, the satellite and the ring must periodically experience very close encounters. In fact, perturbations by 1980S27 act to increase the eccentricity of the F Ring and $\Delta r$ is reduced to $+ 47 \pm 142$ km (Borderies et al. 1983*a*). Here, the uncertainty in $\Delta r$ has been estimated from the uncertainties in the orbital elements and no account has been taken of the effect of these uncertainties on the variation of the eccentricity.

The period between close encounters is largely determined by $J_2$ and is $\approx 18$ yr. Taking the figures for $\Delta r$ at face value, it would appear that every 18 yr the satellite may enter the ring. I consider this to be unlikely. Neglecting the gravitational field of the satellite, I calculate that the relative velocity of the satellite and the ring particles at closest approach is $39 \pm 14$ m s$^{-1}$. This is comparable with the escape velocity (38 m s$^{-1}$) of the isolated satellite (the satellite is close to the Roche limit and so the actual escape velocity will vary



with position on the surface of the satellite, and in places will be considerably less than this value; see chapter by Weidenschilling et al.). If the satellite and the ring orbits intersect, then particles would be swept onto the satellite surface intermittently for a period as long as 2 yr, and this catastrophe would be repeated every 18 yr. If the satellite has an energy absorbing regolith, then I would not expect those particles that impinge on the satellite to survive. However, it is probably significant that $\Delta r$ is comparable with the satellite radius. I would guess that either the mechanism that acts to increase the eccentricity of the ring switches off when $\Delta r$ is small, or the ring is eventually destroyed. We might ask what is special about the F Ring and its inner guardian. The values of $m_s/M$ and $\Delta a/a$ are not markedly different from those values suggested for the Uranian rings (Goldreich and Tremaine 1979*a*). Perhaps the eccentricities of the Uranian rings are limited by close encounters with their guardians.

## III. APSE AND NODE ALIGNMENT

Several types of eccentric rings are now known to exist in the solar system. Rings with forced eccentricities associated with Lindblad resonances have been found in Saturn's rings (Smith et al. 1981, 1982). If $p = 0$ in Eq. (37), then $\dot{\tilde{\omega}} = n'$ and the line of apses rotates with the perturbing satellite. The eccentric Saturnian ring at $1.29 R_s$ is locked in a $p = 0$ Lindblad resonance with Titan (Porco et al. 1983). In terms of the wave description (see Fig. 7), the ring contains a single wave and the resultant shape is an ellipse with Saturn at one focus. If $p = 1$, then the ring contains two waves and the resultant shape is a non-Keplerian ellipse centered on the planet (see Figs. 10 and 11 in Sec. II.C). As predicted by Goldreich and Tremaine (1978*b*), particles in the outer edge of the Saturnian B Ring are observed to be locked in a $p = 1$ Lindblad resonance with Mimas (Smith et al. 1981, 1982).

The eccentric Uranian rings, the eccentric Saturnian rings at 1.45 $R_s$ and in the Maxwell gap, and the Saturnian F Ring have free eccentricities, and their precession rates are largely determined by the dynamical oblateness of the planet $J_2$. The rings which are wide enough to be resolved, and whose geometry is well determined (the $\alpha$, $\beta$ and $\epsilon$ Uranian rings and the Saturnian rings at 1.29 $R_s$ and 1.45 $R_s$), all have markedly nonuniform widths. In all cases, the widths are a minimum at pericenter and a maximum at apocenter (see Fig. 16).

The variation in width of these rings implies either that there is a variation in eccentricity across the ring (Nicholson et al. 1978) or that the pericenters of the particle orbits are systematically misaligned, or both (Dermott and Murray 1980). We define the mean eccentricity gradient of the ring $g_r$ by

$$g_r = a \frac{\delta e}{\delta a} \tag{69}$$

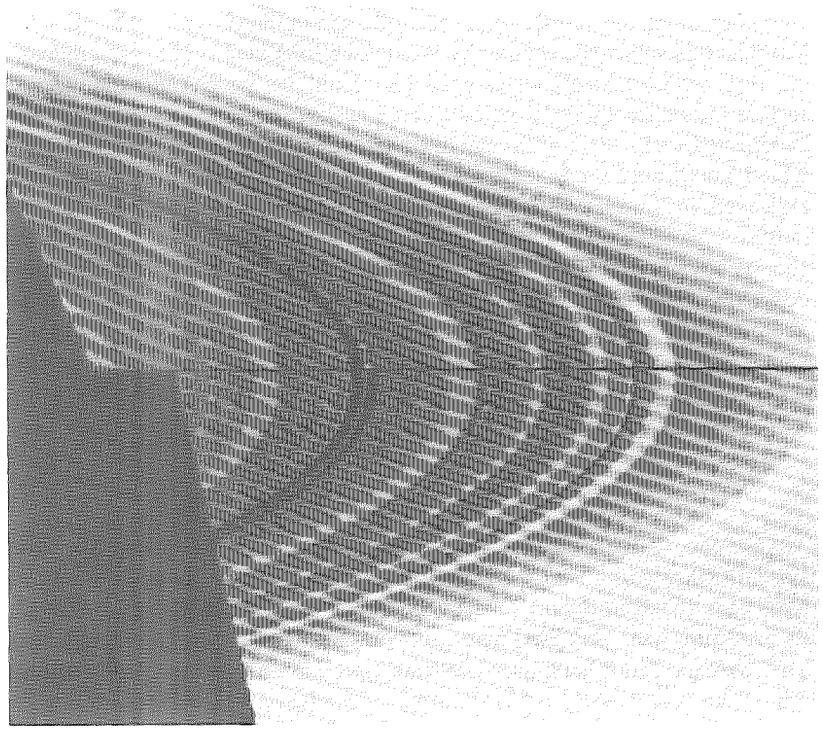

Fig. 16. Composite image of Saturn's C Ring. The horizontal line through the center marks the border between the two images; at the top is shown the trailing ansa of the rings, and at the bottom the leading ansa. The dark gap in the center of both images contains a narrow ring which is clearly both eccentric and of nonuniform width. (Image courtesy of JPL/NASA.)

where $\delta e$ and $\delta a$ are the differences in the eccentricities and the semimajor axes of the Keplerian orbits that define the inner and outer edges of the ring. If the pericenters are aligned, then the variation of the radial ring width $W$ with the true anomaly $f$ is given by

$$W = \delta a[1 - (g_r + e)\cos f] \,. \tag{70}$$

Since, if $e << 1$, the orbital radius $r$ varies as

$$r = a(1 - e\cos f) \,, \tag{71}$$

it follows that the harmonic variations of $W$ and $r$ are in phase and that $W$ varies linearly with $r$ (Nicholson et al. 1978). Any departure from linearity would imply a misalignment of pericenters. For the Uranian $\epsilon$ Ring, at least, this misalignment must be $< 0.^{\circ}2$ (Dermott and Murray 1980). Since $W$ cannot



TABLE III

Eccentric Rings of Nonuniform Width

| Planet | Ring | <W> (km) | $e$ x10$^4$ | $J_2(B/a)^5$ x10$^4$ | $g_r$ |
|---|---|---|---|---|---|
| Uranus[a] | $\alpha$ | 7.5 | 7.2 | 2.3 | 0.35 |
| Uranus[a] | $\beta$ | 7.8 | 4.5 | 2.1 | 0.35 |
| Uranus[a] | $\epsilon$ | 58 | 79.2 | 1.2 | 0.65 |
| Saturn[b] | 1.29 $R_s$ | 25 | 2.7 | 46.9 | 0.35 |
| Saturn[c] | 1.45 $R_s$ | 69 | 3.9 | 26.1 | 0.55 |

[a]Data from chapter by Elliot and Nicholson in this book.
[b]Data from Porco et al. (1983).
[c]Data from Esposito et al. (1983).

be negative (the particle orbits cannot intersect), we must have $|g_r + e| < 1$. However, it is interesting and probably significant that all the observed values of $g_r$ are positive and all are close to the critical value of unity (see Table III).

If the pericenters precessed under the influence of $J_2$ alone, then the differential precession rate across a ring would be

$$\left(\frac{\mathrm{d}\dot{\tilde{\omega}}}{\mathrm{d}a}\right)_J = \frac{-21}{4}\,\frac{n}{a}\,J_2\left(\frac{B}{a}\right)^2 \,. \tag{72}$$

Thus, if no other forces acted, the pericenters would rapidly disperse.

### A. Self-gravitation.

Goldreich and Tremaine (1979*a*,*b*) consider that apse alignment is maintained by the self-gravitation of the ring particles. The contribution of the self-gravitation of the ring to $\mathrm{d}\dot{\tilde{\omega}}/\mathrm{d}a$, which arises from the variation of the radial forces acting on the particles with true anomaly, is given by

$$\left(\frac{\mathrm{d}\dot{\tilde{\omega}}}{\mathrm{d}a}\right)_r = \beta\,\frac{na^3\sigma_r}{M<W>^2} \tag{73}$$

where, for most mass distributions,

$$\beta \approx \frac{3\pi<W>g_r}{ae} \,. \tag{74}$$

If

$$\left(\frac{\mathrm{d}\dot{\tilde{\omega}}}{\mathrm{d}a}\right)_J + \left(\frac{\mathrm{d}\dot{\tilde{\omega}}}{\mathrm{d}a}\right)_r = 0 \,, \tag{75}$$

then

$$g_r \approx +2.3\, e\langle W\rangle J_2 \left(\frac{B}{a}\right)^5 \frac{\rho_b}{\sigma_r} \tag{76}$$

where $\rho_b$ is the density of the planet. Thus, knowledge of the ring geometry yields an estimate of the mean surface mass density $\sigma_r$ of the ring. Note that self-gravity only acts to align the pericenters if the eccentricity gradient $g_r$ is positive and the radial forces are a maximum at pericenter. This is in accord with the observations. The surface mass densities of the Saturnian rings estimated from Eq. (76) are also in accord with independent estimates based on the relation between optical depth and surface mass density established from both the radial wavelengths of density waves and the scattering of the Voyager 1 radio signal (Borderies et al. 1982*a*; see also the chapter by Elliot and Nicholson in this book).

The self-gravitation model of apse alignment has now been extended to node alignment (Borderies et al. 1982*a*; Yoder 1982). The analysis predicts that if the self-gravitation of the ring alone acts to align the apses and the nodes, then we must have

$$\frac{\delta i}{i} = \frac{\delta e}{e} \tag{77}$$

where $\delta i$ is the variation of the inclination of the particle orbits across the ring. Yoder (1982) has also shown that the configuration of aligned pericenters and nodes is stable against small displacements. An eccentric ring is stable even if its inclination is zero, but a ring with an appreciable inclination is only stable if it is also eccentric (Yoder 1982).

### B. Embedded Rings.

The eccentric Saturnian rings at 1.29 $R_s$ and 1.45 $R_s$ have special locations. In both cases, the rings are very close to the outer edges of the clear gaps in which they lie (Porco et al. 1983; Esposito et al. 1983). In the case of the 1.45 $R_s$ ring, the particles in the outer edge of the eccentric ring may even brush the surrounding disk at their apocenters (Esposito et al. 1983). These configurations may not be fortuitious. The closeness of the rings to the surrounding disk leaves little room for shepherding satellites. However, the ring particle orbits will be perturbed at each close encounter with the disk. Perhaps this interaction results in shepherding action.

The location of the rings may also have some other significance. The contribution of a circular disk to the differential precession of a nearby narrow eccentric ring is given by

$$\left(\frac{d\dot{\tilde{\omega}}}{da}\right)_d = \frac{(1+\gamma)\, n a^3 \sigma_d}{M \Delta a^2} \tag{78}$$



(cf. Eq. 73) where

$$\gamma = \frac{3}{4} g_d^2 - \frac{1}{2} g_d g_r + \frac{5}{8} g_d^4 - \frac{1}{2} g_d^3 g_r + \ldots \tag{79}$$

where $g_d$ $(= ae/\Delta a)$ is the eccentricity gradient between the ring and the inner edge of the circular disk, $\Delta a (<0)$ is the corresponding difference in the semimajor axes and $\sigma_d$ is the surface mass density of the disk. Regardless of the sign of $g_r$, $(d\dot{\tilde{\omega}}/da)_d$ is only positive if the eccentric ring is close to the inside edge of the disk. That this is the case for the Saturnian rings suggests that the disk may have a role in their apse alignment. Using Eqs. (72), (78) and (79), I calculate that even if the rings were massless ($\sigma_r = 0$), $d\dot{\tilde{\omega}}/da$ would be zero where

$$\Delta a = -56 \left(\frac{\sigma_d}{100 \text{ g cm}^{-2}}\right)^{\frac{1}{2}} \text{km} \tag{80}$$

in the case of the 1.45 $R_s$ ring, and where

$$\Delta a = -42 \left(\frac{\sigma_d}{100 \text{ g cm}^{-2}}\right)^{\frac{1}{2}} \text{km} \tag{81}$$

in the case of the 1.29 $R_s$ ring (neglecting the contribution of Titan to $d\dot{\tilde{\omega}}/da$). Thus, the disk may partly determine the local eccentricity gradients of the outer edges of the rings; these local gradients may even be negative. This might imply that the eccentricity gradients at the edges may differ appreciably from the observed mean eccentricity gradients, and may be equal to those critical values for which the angular momentum flux rates are zero and the edges are sharp (Borderies et al. 1982*b*, 1983*b*).

### C. Precessional Pinch.

Dermott and Murray (1980) pointed out that by itself self-gravitation does not explain why all the observed values of $g_r$ are close to unity. If $g_r$ is determined by three presumably independent parameters of the ring ($e$, $\langle W\rangle$ and $\sigma_r$), then it is unreasonable to expect those quantities to be always such that $g_r \approx 0.5$ (see Table III). They argued that the ring particles may be close-packed at pericenter and that close-packing may prevent differential precession. Figure 17 gives an heuristic description of how differential precession, particle collisions, and self-gravitation acting together always transform a narrow eccentric ring of uniform width into a ring with a large positive eccentricity gradient and aligned pericenters. Equilibrium (Fig. 17*d*) is only reached when the particles are so close together at pericenter that the ring width there cannot be reduced any further. Since differential precession always acts to reduce the ring width, it must then cease.

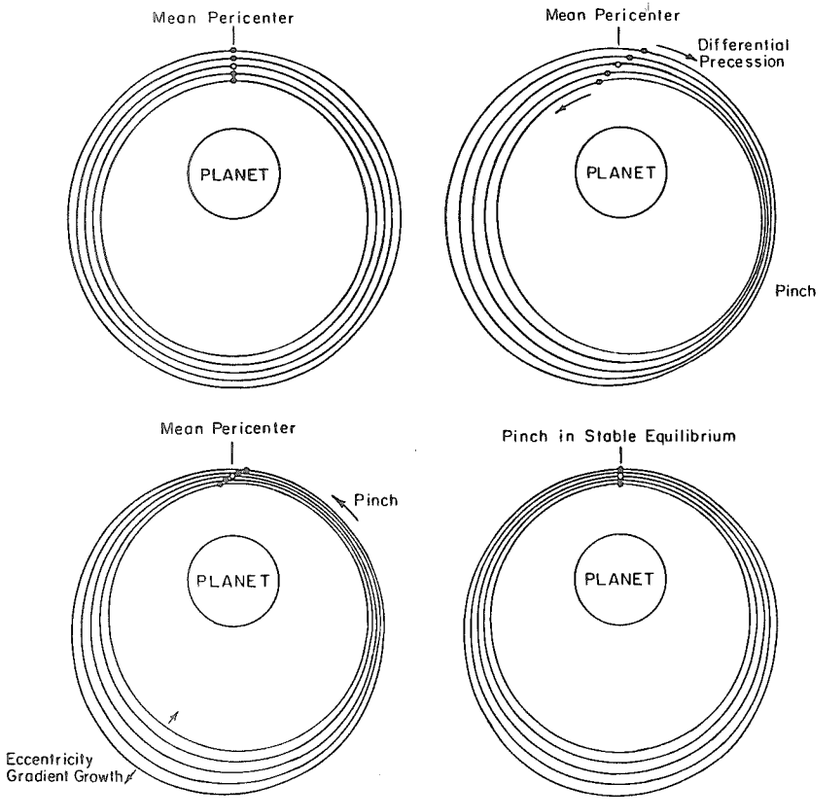


Fig. 17. Possible evolution of a narrow eccentric ring due to differential precession. (a) Initially the pericenters are aligned and the ring width is uniform. (b) Differential precession produces a harmonic variation of width with the pinch ($W_{min}$) located before pericenter ($f \simeq -\pi/2$). The pericenters of the eccentric orbits are denoted by filled circles; the mean pericenter of the ring by an open circle. As the pericenters separate, $W_{min}$ decreases. Dermott and Murray (1980) contend that close packing of particles at the pinch prevents $W_{min}$ from being reduced to zero. (c) The further evolution of the ring is now determined by self-gravitation, resulting in the growth of a positive eccentricity gradient. As the eccentricity gradient increases, the pinch moves in a prograde sense towards pericenter. (d) Only at pericenter is the pinch in stable equilibrium.

The only alternative to this argument is to allow that $e$, $<W>$, $\sigma_r$ and $g_r$ are not independent parameters (Dermott and Murray 1980). The coupled evolution of these parameters has now been solved by Borderies et al. (1983*c*). In their model, self-gravitation is always responsible for the alignment of the pericenters, and evolution of the parameters only ceases when close-packing of the particles at pericenter limits the growth of the mean eccentricity $e$.



### D. Sharp Edges.

The particle dynamics of an eccentric ring with a large eccentricity gradient are quite different from those of a circular ring, because both the relative velocities of the particles and their collision frequencies can vary markedly with true anomaly (Dermott and Murray 1980). The radial variation of angular frequency $\dot{f}$ for a ring with aligned pericenters is given by

$$\frac{d\dot{f}}{dr} = -\frac{3}{2}\frac{n}{a}\frac{\left(1-\frac{4}{3}g_r\cos f\right)}{(1-g_r\cos f)} \tag{82}$$

and, if $g_r > 3/4$, then the angular velocity gradient at pericenter is positive. Borderies et al. (1982*b*) have shown that this change of sign has a profound effect on the angular momentum transfer rate due to particle collisions, and probably accounts for the existence of rings with very sharp edges. Their model is shown in Fig. 10 (see Sec. II.C).

Using the fluid approximation (Eq. 4), Borderies et al. have shown that the net angular momentum flow rate is zero and the ring edge is sharp when the magnitude of the eccentricity gradient at the ring edge is $(3/4)^{\frac{1}{2}}$. [Note that in their model the fundamental quantity is the azimuthal variation of the radial width of adjacent streamlines, and that this is determined by the eccentricity gradient $g_r$ alone only when the pericenters are aligned (see Dermott and Murray 1980, and Eq. 70). Their more general treatment also allows for the azimuthal variation of radial width associated with misalignment of pericenters (this effect is shown in Fig. 17). For very narrow rings, the latter effect can be dominant.] A more sophisticated analysis, using the Boltzmann equation, shows that the critical eccentricity gradient varies with the mean optical depth of the ring $\tau$ (Borderies et al. 1983*b*). For $\tau > 3$, the critical gradient is close to the fluid limit 0.866, but the critical gradient decreases with $\tau$ and for $\tau \approx 0.25$ it is as low as 0.5. The local eccentricity gradient, $ade/da$, is strongly radially dependent near any Lindblad resonance (see Eq. 38) (and, perhaps, near the inner edge of a disk). For this reason, Borderies et al. (1982*b*) consider that the sharp edges of all rings in the solar system are probably associated with Lindblad resonances.

## IV. HORSESHOE ORBITS

Dermott et al. (1979) proposed that each narrow ring contains a small satellite that maintains solid particles in stable, horseshoe orbits about its Lagrangian equilibrium points (Fig. 18). The case for which the ring-satellite has zero eccentricity can be studied by considering the Jacobi integral. In a rotating reference frame in which the satellite is fixed, this integral is (Brown 1911)

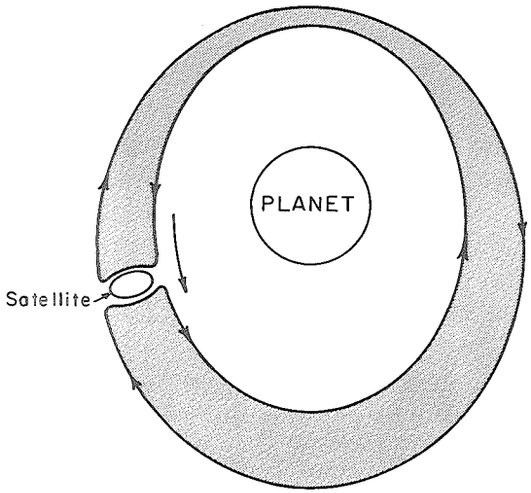


Fig. 18. Ring model of Dermott et al. (1979); each ring contains a small satellite which maintains particles in horseshoe orbits. Loose solid particles leave the satellite surface and enter orbits closely similar to that of the satellite (which can be both eccentric and inclined to the equatorial plane of the planet). The gravitational force of the satellite in a 1:1 resonance with the ring particles provides the critical phenomenon needed to define a narrow ring. (Figure copyright of *Nature*, MacMillan Journals Ltd.)

$$\frac{2}{r} + r^2 + \frac{m}{M}\left(\frac{2}{\Delta} + \Delta^2\right) = V^2 + C \qquad (83)$$

where $r$ is the distance of the particle from the center of the planet, $\Delta$ is the distance from the satellite, and $V$ is the speed in the rotating reference frame (Fig. 19). The unit of distance is the separation of the satellite from the center of the planet, and the unit of time is chosen such that the mean motion $n$ of the satellite is given by

$$n^2 = 1 + m/M \ . \qquad (84)$$

This requires $GM = 1$. The curves $V^2 = 0$ for a range of values of the Jacobi constant $C$ are called zero-velocity curves, and define regions of the plane within which the particle is confined to move.

The shapes and widths of these curves are very good guides to the geometry of the actual particle paths. Dermott and Murray (1981*a*) have shown that, if $(m/M)^{\frac{1}{6}} << 1$, there is a close correspondence between a particle's path and its associated zero-velocity curve. If a particle is moving in a near-circular orbit, and the radial displacement of its associated zero-velocity curve from the unit circle is $W_z$, then the radial displacement of the particle path at the same longitude is $2W_z$; if the particle orbit has a small eccentricity, then this statement applies to the motion of the guiding center.



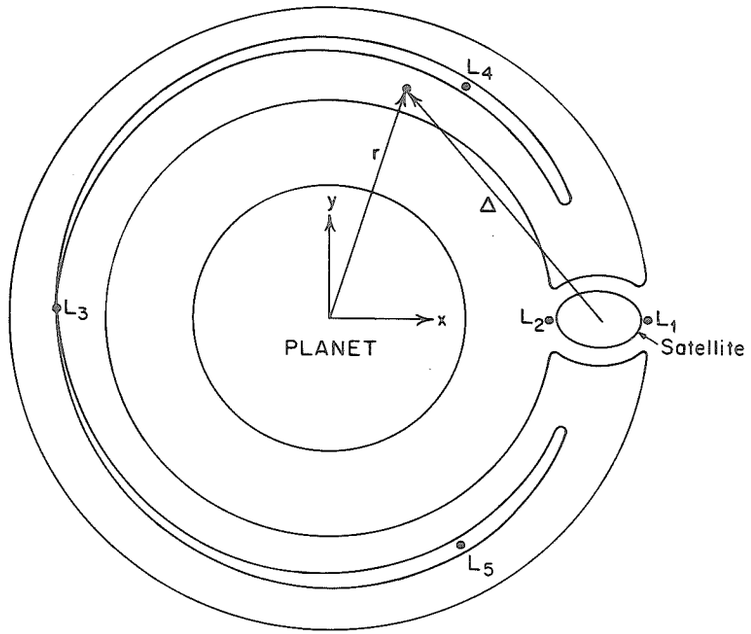


Fig. 19. Schematic diagram showing the Lagrangian equilibrium points and the critical zero-velocity curves. The critical horseshoe curve actually passes through $L_1$ and $L_2$ and the critical tadpole curve passes through $L_3$. Horseshoe orbits will exist between these two extremes. The rectangular coordinate frame is centered on the planet and corotates with the satellite.

Tadpole orbits encompass either $L_4$ or $L_5$ alone, whereas horseshoe orbits encompass $L_3$, $L_4$ and $L_5$ (Fig. 19). In most of the past work on the three-body problem, emphasis has been placed on the tadpole solutions, since these describe the motion of the Trojan asteroids with respect to Jupiter. Until the Voyager encounters with Saturn, examples of horseshoe orbits in the solar system were unknown. Dermott et al. (1979, 1980) pointed out that for two reasons we must expect horseshoe orbits in the solar system to be associated only with very small satellites. First, the ratio of the widths of those regions where, respectively, tadpole alone and tadpole and horseshoe orbits are possible is $\approx (m/M)^{\frac{1}{6}}$, and it follows that the horseshoe orbit region is only dominant if $(m/M)^{\frac{1}{6}} << 1$. The second reason obtains from a study of orbital stability.

For motion in a horseshoe orbit it is convenient to write the Jacobi constant $C$ as

$$C = 3 + \alpha \left(\frac{m}{M}\right)^{\frac{2}{3}} \tag{85}$$

where $\alpha$ is a constant $\leq 3^{\frac{4}{3}}$. If we write

$$a = a_s + \Delta a \tag{86}$$

where $a$ and $a_s$ are the semimajor axes of a ring particle and a ring satellite respectively, then

$$\Delta a = 2 \left(\frac{\alpha}{3}\right)^{\frac{1}{2}} \left(\frac{m}{M}\right)^{\frac{1}{3}} a_s \tag{87}$$

and the distance of closest approach of a particle (or its guiding center) to the satellite is

$$y = \frac{2}{\alpha}\left(\frac{m}{M}\right)^{\frac{1}{3}} a_s \tag{88}$$

(Dermott and Murray 1981*a*).

Dermott et al. (1980, 1981*a*) have found by numerical integration of particular cases that the type of path followed by a particle depends on the value of $\alpha$. For large values of $\alpha(>1)$ the particles either strike the satellite or are scattered, but for small values of $\alpha$ $(<1)$ the particles are apparently repelled by the satellite and motion in horseshoe orbits is possible (for a simple discussion of the dynamics involved see Dermott et al. 1979). The nature of the path changes dramatically as $\alpha$ is reduced, and for very small values of $\alpha$ the horseshoe paths are almost perfectly symmetric with respect to the unit circle.

If we write

$$\left|\frac{\Delta a_0}{a_s}\right| - \left|\frac{\Delta a_j}{a_s}\right| = \pm \left(\frac{m}{M}\right)^n \tag{89}$$

where the subscript $j$ refers to the number of consecutive encounters with the satellite that the particle experiences, then we find that $n$ increases to values $>0.7$ $(j=1)$ and $\approx 1.2$ $(j=2)$ as $\alpha$ decreases to $<0.2$ (Fig. 20). Thus, for small values of $\alpha$ the orbits are near-periodic and $\Delta a_0$ and $\Delta a_2$ are equal to order $m/M$. This symmetry is not a property of the circular orbit case alone. Fig. 20 shows that there is no substantial difference between the cases of circular and eccentric orbits.



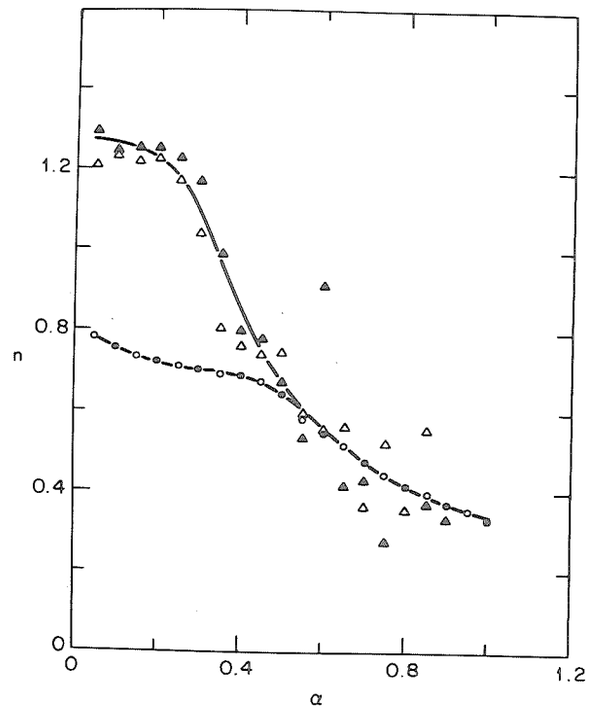


Fig. 20. Summary of horseshoe paths. $n$ is a measure of the symmetry of the horseshoe path (see Eq. 89). $\alpha$ is the impact parameter, proportional to $\Delta a^2$. The circular points refer to changes in the semimajor axis $a$ of the particle orbit after a single encounter with the satellite: filled circles refer to the circular orbit case ($e_s = 0$, where $e_s$ is the eccentricity of the satellite orbit); open circles refer to the elliptical orbit case with $e_s = 0.01$. The triangular points refer to the total change in $a$ after two consecutive encounters: filled triangles, $e_s = 0$; open triangles, $e_s = 0.01$.

The effect on the horseshoe orbit of a ring particle by an external force due, for example, to Poynting-Robertson light drag can now be understood. If $\alpha$ is small, then $\Delta a_0$ and $\Delta a_2$ are always equal; drag forces have little influence on the encounter dynamics. Therefore, if the ring were very narrow and the magnitudes of the drag forces acting on the particle were the same in both halves of the horseshoe path, then the orbital decay of the particle achieved in one half of the path would in effect be cancelled by that achieved in the other half (Fig. 21). Since the drag force extracts angular momentum from the system, some orbital decay would of course occur, but the satellite would supply angular momentum to the particle to maintain the 1:1 resonance and the orbit of the ring particle and the satellite would decay together at some rate $r$ times less than that of an unconstrained particle, where

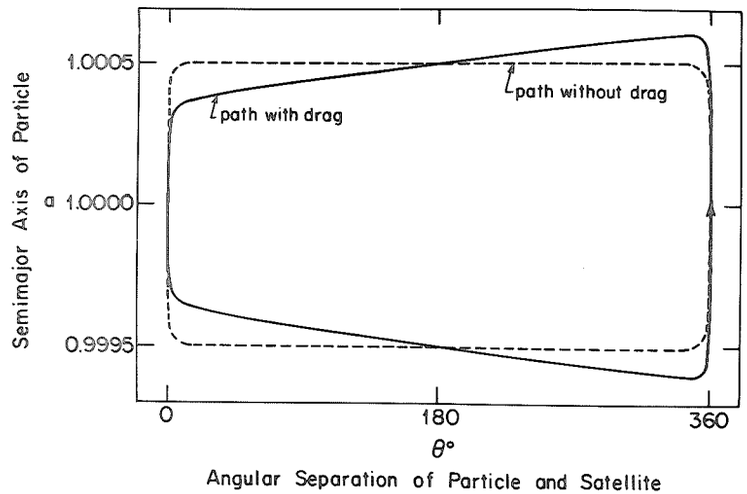


Fig. 21. Path of a particle moving in a horseshoe orbit around a ring-satellite of mass ratio $m/M = 10^{-6}$ (circular orbit case). The dashed line refers to the particle path in the absence of drag, and the solid line shows the effect of an external drag force. Since $\alpha < 0.2$, both paths are highly symmetric about the line $a = 1$ and both paths are closed (to order $m/M$). Thus, even in the presence of drag, the particle orbit is stable; the ring-satellite provides the energy and angular momentum needed to maintain the 1:1 resonance.

$$r \approx \frac{m_r}{m_s + m_r} \tag{90}$$

(Dermott et al. 1979, 1980; Dermott 1981*a*). Thus, even if a ring consisted of very small particles ($d << 0.1$ cm), if $m_s >> m_r$ then Poynting-Robertson light drag acting over times comparable with the age of the solar system would not result in significant orbital decay or ring spreading. However, second-order effects associated with the variation of the magnitude of the mean drag force with distance from the planet may not be negligible.

From Fig. 21, we see that orbital decay on the inside of the horseshoe acts to increase the width $W$ of the path, whereas that on the outside acts to decrease it. If $\dot{a} < 0$ and $\mathrm{d}|a|/\mathrm{d}a < 0$, then one might expect $W$ to increase with time. However, since the particle's orbital period decreases with increasing $a$ (Kepler's third law), the particle spends a greater time on the outside than on the inside of the horseshoe path, and the sign of $\dot{W}$ is found to depend on the magnitude of $\mathrm{d}|\dot{a}|/\mathrm{d}a$. If $\dot{a} = -k^2 a^n$, where $k$ is a constant, then $\dot{W}/W = (3+n)(\dot{a}/a)$ and, if $n > -3$, then $\dot{W} < 0$ and the particles are driven towards $L_4$ and $L_5$. From Eq. (8), we see that this is the case for the Poynting-Robertson light drag.



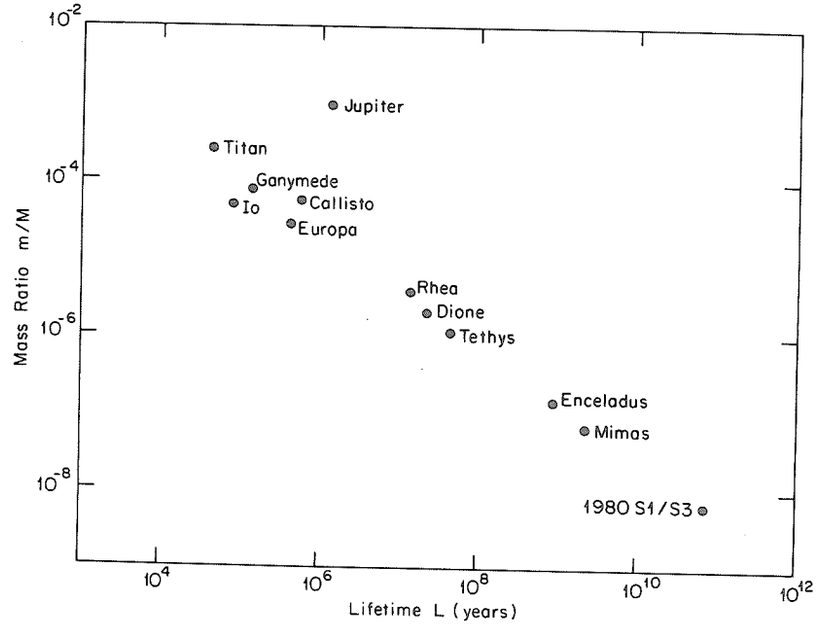


Fig. 22. Values of $L$ for solar system bodies. If the evolution of the semimajor axis of a small satellite moving in a horseshoe orbit due to encounters with a primary or more massive coorbital satellite can be described by a random-walk process, then the lifetime $L$ of the small satellite can be estimated from the mass ratio $m/M$, where $m$ is the mass of the primary satellite and $M$ is the mass of the planet. Horseshoe orbits may be associated only with very small or young primary satellites.

If Eq. (89) were sufficient to describe the effects of particle and satellite encounters, then I would expect particles to be lost from horseshoe orbits due to a random walk of the quantity $|\Delta a_0| - |\Delta a_2|$. If $n = 1$ in Eq. (89), then this would occur on a time scale

$$L \approx \frac{T}{(m/M)^{\frac{5}{3}}} \tag{91}$$

where $T$ is the orbital period of the satellite (Dermott et al. 1980). Values of $L$ for various bodies in the solar system are shown in Fig. 22. On this basis, Dermott et al. (1980) suggested that very small satellites which lie outside the Roche zone may be associated with narrow rings of primordial material that they have yet to accrete. Their numerical investigations and those of Dermott and Murray (1981*a*) were not very extensive. Thus Eq. (91) cannot be regarded as well supported. Nevertheless, it is encouraging that those satellites since discovered to be associated with companions in horseshoe orbits, have lifetime $L > 5 \times 10^9$ yr; these are the coorbital satellites 1980S1 and 1980S3

(Smith et al. 1981, 1982) and Mimas (Simpson et al. 1980; Van Allen et al. 1980; Stone and Miner 1982; Van Allen 1982).

It is natural to suggest that the coorbital satellites 1980S1 and 1980S3 are direct collision products, but I consider this unlikely. Dermott and Murray (1981*a*) have shown that high-$\alpha$ orbits are very unstable. A satellite could not remain in such an orbit for long without either being scattered away from the more massive satellite or colliding with it. Since any objects which leave the surface of the main satellite must, if they move in horseshoe orbits at all, move in high-$\alpha$ orbits, it is improbable that the present orbital configuration, characterized by a very low $\alpha$ value (0.025), was formed in that way. Similar arguments apply to the formation of the coorbital satellites of Mimas, Dione, and Tethys. If collisions have had a role in the formation of coorbital satellites, then I consider that the formation of a narrow ring of coorbital debris out of which the coorbital satellites then accrete is a necessary intermediate step. I can see no other way of placing large quantities of material in the low-$\alpha$ orbits necessary for orbital stability and satellite survival (Dermott and Murray 1981*b*; Yoder et al. 1983).

The existence of satellites in horseshoe orbits lends support to the horseshoe orbit ring model. However, other observations argue against it. In particular, occultation data show that the structure of some of the Uranian rings is highly complex. Such asymmetric profiles could not possibly be modeled by a ring which contains a single satellite. Whether small satellites exist in Saturn's rings that maintain rings of particles on horseshoe paths is not known, but I would argue that they probably do.

*Acknowledgment*. This research was supported by the National Aeronautics and Space Administration.

## REFERENCES

Aksnes, K. 1977. Quantitative analysis of the Dermott-Gold theory for Uranus's rings. *Nature* 269:783.

Borderies, N., Goldreich, P., and Tremaine, S. 1982*a*. Precession of inclined rings. *Icarus* (in press).

Borderies, N., Goldreich, P., and Tremaine, S. 1982*b*. Sharp edges of planetary rings. *Icarus* (in press).

Borderies, N., Goldreich, P. and Tremaine, S. 1983*a*. The variations in eccentricity and apse precession rate of a narrow ring perturbed by a close satellite. *Icarus* 53:84–89.

Borderies, N., Goldreich, P. and Tremaine, S. 1983*b*. Perturbed particle disks. *Icarus* 55:124–132.

Borderies, N., Goldreich, P. and Tremaine, S. 1983*c*. The dynamics of elliptical rings. *Icarus* (in press).

Brahic, A. 1977. Systems of colliding bodies in a gravitational field. I. Numerical simulation of the standard model. *Astron. Astrophys.* 54:895–907.

Brahic, A. 1982. The rings of Uranus. In *Uranus and the Outer Planets*, ed. G. Hunt (Cambridge: Cambridge Univ. Press), pp. 211–236.

Brown, E. W. 1911. On a new family of periodic orbits in the problem of three bodies. *Mon. Not. Roy. Astron. Soc.* 71:438–454.



Burns, J. A., Lamy, P. L., and Soter, S. 1979. Radiation forces on small particles in the solar system. *Icarus* 40:1–48.

Burns, J. A., Showalter, M. R., Cuzzi, J. N., and Pollack, J. B. 1980. Physical processes in Jupiter's ring: Clues to its origin by Jove! *Icarus* 44:339–360.

Clarke, J. T. 1982. Detection of auroral hydrogen Lyman-alpha emission from Uranus. *Astrophys. J.* 263:L105–L109.

Cook, A. F., and Franklin, F. A. 1964. Rediscussion of Maxwell's Adams prize essay on the stability of Saturn's rings. *Astron. J.* 69:173–200.

Cuzzi, J. N. 1982. Mysteries of the ringed planets. *Nature* 300:485–486.

Cuzzi, J. N., Lissauer, J. J., and Shu, F. H. 1981. Density waves in Saturn's rings. *Nature* 292:703–707.

Dermott, S. F. 1981*a*. The origin of planetary rings. *Phil. Trans. Roy. Soc. London.* A303: 261–279.

Dermott, S. F. 1981*b*. The braided F ring of Saturn. *Nature* 290:54–57.

Dermott, S. F., and Gold. T. 1977. The rings of Uranus: theory. *Nature* 267:590–593.

Dermott, S. F., Gold, T., and Sinclair, A. T. 1979. The rings of Uranus: Nature and origin. *Astron. J.* 84:1225–1234.

Dermott, S. F., and Murray, C. D. 1980. Origin of the eccentricity gradient and the apse alignment of the $\epsilon$ ring of Uranus. *Icarus* 43:338–349.

Dermott, S. F., and Murray, C. D. 1981*a*. The dynamics of tadpole and horseshoe orbits. I. Theory. *Icarus* 48:1–11.

Dermott, S. F., Murray, C. D., and Sinclair, A. T. 1980. The narrow rings of Jupiter, Saturn and Uranus. *Nature* 284:309–313.

Dermott, S. F., and Murray, C. D. 1981*b*. The dynamics of tadpole and horseshoe orbits. II. The coorbital satellites of Saturn. *Icarus* 48:12–22.

Dermott, S. F., and Murray, C. D. 1983. Kirkwood gaps in the distribution of the asteroids. I. The 3:1 resonance with Jupiter. In preparation.

Dermott, S. F., Murray, C. D., and Williams, I. P. 1984. Drag forces in the three-body problem and the formation of coorbital satellites. In preparation.

Elliot, J. L. 1979. Stellar occultation studies of the solar system. *Ann. Rev. Astron. Astrophys.* 17:445–475.

Elliot, J. L., Dunham, E. W., and Mink, D. J. 1977. The rings of Uranus. *Nature* 267:328–330.

Esposito, L. W., Borderies, N., Goldreich, P., Cuzzi, J. N., Holberg, J. B., Lane, A. L., Pomphrey, R. B., Terrile, R. J., Lissauer, J. J., Marouf, E. A., and Tyler, G. L. 1983. The eccentric ringlet in the Huygens gap at 1.45 Saturn radii: Multi-instrument Voyager observations. *Science* 222:57–60.

Fanale, F. P., Veeder, G., Matson, D. L., and Johnson, T. V. 1980. Rings of Uranus: Proposed model is unworkable. *Science* 208:626.

Freedman, A. P., Tremaine, S., and Eliot, J. L. 1983. Weak dynamical effects in the Uranian ring system. *Astrophys. J.* In press.

French, R. G., Elliot, J. L., and Allen, D. A. 1982. Inclinations of the Uranian rings. *Nature* 298:827–829.

Gehrels, T., Baker, L. R., Beshore, E., Bleman, C., Burke, J. J., Castillo, N. D., Dacosta, B., Degewij, J., Doose, L. R., Fountain, J. W., Gotobed, G., Kenknight, C. E., Kingston, R., McLaughlin, G., McMillan, R., Murphy, R., Smith, P. H., Stoll, C. P., Strickland, R. N., Tomasko, M. G., Wijesinghe, M. P., Coffeen, D. L., and Esposito, L. 1980. Imaging photopolarimeter on Pioneer Saturn. *Science* 207:434–439.

Goldreich, P. 1965. An explanation of the frequent occurrence of commensurable mean motions in the solar system. *Mon. Not. Roy. Astron. Soc.* 130:159–181.

Goldreich, P., and Nicholson, P. 1977. The revenge of tiny Miranda. *Nature* 269:783–785.

Goldreich, P., and Tremaine, S. 1978*a*. The velocity dispersion in Saturn's rings. *Icarus* 34:227–239.

Goldreich, P., and Tremaine, S. 1978*b*. The formation of the Cassini Division in Saturn's rings. *Icarus* 34:240–253.

Goldreich, P., and Tremaine, S. 1978*c*. The excitation and evolution of density waves. *Astrophys. J.* 222:850–858.

Goldreich, P., and Tremaine, S. 1979*a*. Towards a theory for the uranian rings. *Nature* 277:97–99.
Goldreich, P., and Tremaine, S. 1979*b*. Precession of the $\epsilon$ ring of Uranus. *Astron. J.* 84:1638–1641.
Goldreich, P., and Tremaine, S. 1979*c*. The excitation of density waves at the Lindblad and corotation resonances by an external potential. *Astrophys. J.* 233:857–871.
Goldreich, P., and Tremaine, S. 1980. Disk-satellite interactions. *Astrophys. J.* 241:425–441.
Goldreich, P., and Tremaine, S. 1981. The origin of the eccentricities of the rings of Uranus. *Astrophys. J.* 243:1062–1075.
Goldreich, P., and Tremaine, S. 1982. The dynamics of planetary rings. *Ann. Rev. Astron. Astrophys.* 20:249–283.
Gradie, J. 1980. Rings of Uranus: Proposed model is unworkable. *Science* 208:625–626.
Greenberg, R. 1973. Evolution of satellite resonances by tidal dissipation. *Astron. J.* 78:338–346.
Greenberg, R. 1983. The role of dissipation in shepherding of ring particles. *Icarus* 53: 207–218.
Greenberg, R. 1984. Resonances in the Saturn system. In *Saturn,* eds. T. Gehrels and M. S. Matthews (Tucson: Univ. Arizona Press). In press.
Harris, A. W., and Ward, W. R. 1982. Dynamical constraints on the formation and evolution of planetary bodies. *Ann. Rev. Earth Planet. Sci.* 10:61–108.
Harris, A. W., and Ward, W. R. 1983. On the radial structure of planetary rings. Proceedings of *I.A.U. Colloquium 75 Planetary Rings,* ed. A. Brahic, Toulouse, France, Aug. 1982.
Hénon, M. 1981. A simple model of Saturn's rings. *Nature* 293:33–35.
Hénon, M. 1983. A simple model of Saturn's rings-revisited. Proceedings of *I.A.U. Colloquium 75 Planetary Rings,* ed. A. Brahic, Toulouse, France, Aug. 1982.
Holberg, J. B., Forrester, W. T., and Lissauer, J. J. 1982. Identification of resonance features within the rings of Saturn. *Nature* 297:115–120.
Hunten, D. M. 1980. Rings of Uranus: Proposed model is unworkable. *Science* 208:625–626.
Ip, W. H. 1980*a*. Physical studies of planetary rings. *Space Sci. Rev.* 26:39–96.
Ip, W. H. 1980*b*. New progress in the physical studies of planetary rings. *Space Sci. Rev.* 26:97–109.
Julian, W. H., and Toomre, A. 1966. Non-axisymmetric responses of differentially rotating disks of stars. *Astrophys. J.* 146:810–832.
Lane, A. L., Hord, C. W., West, R. A., Esposito, L. W., Coffeen, D. L., Sato, M., Simmons, K., Pomphrey, R. B. and Morris, R. B. 1982. Photopolarimetry from Voyager 2: Preliminary results on Saturn, Titan and the rings. *Science* 215:537–543.
Lin , D. N. C., and Bodenheimer, P. 1981. On the stability of Saturn's rings. *Astrophys. J.* 248:L83–L86.
Lin, D. N. C., and Papaloizou, J. 1979. Tidal torques on accretion discs in binary systems with extreme mass ratios. *Mon. Not. Roy. Astr. Soc.* 186:799–812.
Lucke, R. L. 1978. Uranus and the shape of elliptical rings. *Nature* 272:148.
Lukkari, J. 1981. Collisional amplification of density fluctuations in Saturn's rings. *Nature* 292:433–435.
Lynden-Bell, D., and Pringle, J. E. 1974. The evolution of viscous discs and the origin of the nebular variables. *Mon. Not. Roy. Astron. Soc.* 168:603–637.
Matthews, K., Neugebauer, G., and Nicholson, P. D. 1982. Maps of the rings of Uranus at a wavelength of 2.2 microns. *Icarus* 52:126–135.
Nicholson, P. D., Matthews, K., and Goldreich, P. (1982). Radial widths, optical depths and eccentricities of the Uranian rings. *Astron. J.* 87:433–447.
Nicholson, P. D., Persson, S. E., Matthews, K., Goldreich, P., and Neugebauer, G. 1978. The rings of Uranus: Results of the 1978 10 April occultation. *Astron. J.* 83:1240–1248.
Porco, C., Borderies, N., Danielson, G. E., Goldreich, P., Holberg, J. B., Lane, A. L., and Nicholson, P. D. 1983. The eccentric ringlet at 1.29 $R_S$. Proceedings of *I.A.U. Colloquium 75 Planetary Rings,* ed. A. Brahic, Toulouse, France, Aug. 1982.
Safronov, V. S. 1969. *Evolution of the Protoplanetary Cloud and Formation of the Earth and Planets.* Moscow: Nanka. Transl. Israel Program for Scientific Translations, 1972. NASA TTF-677.
Sandel, B. R., Shemansky, D. E., Broadfoot, A. L., Holberg, J. B., Smith, G. R., McConnell, J. C., Strobel, D. F., Atreya, S. K., Donahue, T. M., Moos, H. W., Hunten, D. M., Pomphrey, R. B., and Linick, S. 1982. Extreme ultraviolet observations from the Voyager 2 encounter with Saturn. *Science* 215:548–553.
Showalter, M. R., and Burns, J. A. 1982. A numerical study of Saturn's F Ring. *Icarus* 52:526–544.
Sicardy, B., Combes, M., Brahic, A., Bouchet, P., Perrier, C., and Courtin, R. 1983. The 15 August 1980 occultation by the Uranian system: structure of the rings and temperature of the upper atmosphere. *Icarus* 52:454–472.
Simpson, J. A., Bastian, T. S., Chenette, D. L., McKibben, R. B., and Pyle, K. R. 1980. The trapped radiations of Saturn and their absorption by satellites and rings. *J. Geophys. Res.* 85:5731–5762.
Smith, B. A., Soderblom, L. A., Johnson, T. V., Ingersoll, A. P., Collins, S. A., Shoemaker, E. M., Hunt, G. E., Carr, M. H., Davies, M. E., Cook, A. F., Boyce, J., Danielson, G. E., Owen, T., Sagan, C., Beebe, R. F., Veverka, J., Strom, R. G., McCauley, J. F., Morrison, D., Briggs, G. A., and Suomi, V. E. 1981. Encounter with Saturn: Voyager 1 imaging science results. *Science* 212:163–191.
Smith, B. A., Soderblom, L., Beebe, R., Boyce, J., Briggs, G., Bunker, A., Collins, S. A., Hansen, C. J., Johnson, T. V., Mitchell, J. L., Terrile, R. J., Carr, M., Cook, A. F., Cuzzi, J., Pollack, J. B., Danielson, G. E., Ingersoll, A., Davies, M. E., Hunt, G. E., Masursky, H., Shoemaker, E., Morrison, D., Owen, T., Sagan, C., Veverka, J., Strom, R., and Suomi, V. E. 1982. A new look at the Saturn system : The Voyager 2 images. *Science* 215:504–537.
Stone, E. C., and Miner, E. D. 1982. Voyager 2 encounter with the saturnian system. *Science* 215:499–504.
Synott, S. P., Terrile, R. J., Jacobson, R. A., and Smith, B. A. 1983. Orbit's of Saturn's F Ring and its shepherding satellites. *Icarus* 53:156–158.
Van Allen, J. A. 1982. Findings on rings and inner satellites of Saturn by Pioneer 11. *Icarus* 51:509–527.
Van Allen, J. A., Thomsen, M. F., and Randall, B. A. 1980. The energetic charged particle absorption signature of Mimas. *J. Geophys. Res.* 85:5709–5718.
Van Flandern, T. C. 1979. Rings of Uranus: invisible and impossible? *Science* 204:1076–1077.
Vogt, R. E., Chenette, D. L., Cummings, A. C., Garrard, T. L., Stone, E. C., Schardt, A. W., Trainor, J. H., Lal, N., and McDonald, F. B. 1982. Energetic charged particles in Saturn's magnetosphere: Voyager 2 results. *Science:* 215:577–582.
Ward, W. R. 1981. On the radial structure of Saturn's ring. *Geophys. Res. Lett.* 8:641–643.
Yoder, C. F. 1983. The gravitational interaction between inclined, elliptical rings. Proceedings of *I.A.U. Colloquium 75 Planetary Rings,* ed. A. Brahic, Toulouse, France, Aug. 1982.
Yoder, C. F., Colombo, G., Synnott, S. P., and Yoder, K. A. 1983. Theory of motion of Saturn's coorbiting satellites. *Icarus* 53:431–443.